Plasmodium RON11 triggers biogenesis of the merozoite rhoptry pair and is essential for erythrocyte invasion

David Anaguano[1,2], Opeoluwa Adewale-Fasoro[3,4], Grace S. Vick[2,5], Sean Yanik[3,4], James Blauwkamp[6], Manuel A. Fierro[1,2,#], Sabrina Absalon[6], Prakash Srinivasan[3,4] and Vasant Muralidharan[1,2,*]

[1]Department of Cellular Biology, [2]Center for Tropical and Emerging Global Diseases, University of Georgia, Athens, GA.

[3]Department of Molecular Microbiology and Immunology, and Johns Hopkins Malaria Institute, Johns Hopkins Bloomberg School of Public Health, Baltimore, MD

[4]The Johns Hopkins Malaria Research Institute, Baltimore, MD, 21205, USA.

[5]Department of Infectious Diseases, College of Veterinary Medicine, University of Georgia, Athens, GA.

[6]Department of Pharmacology and Toxicology, Indiana University School of Medicine, Indianapolis IN.

[#]Current address: Department of Biomedical Sciences, College of Veterinary Medicine, Iowa State University, Ames IA

*Corresponding author: vasant@uga.edu

ABSTRACT

Malaria is a global and deadly human disease caused by the apicomplexan parasites of the genus *Plasmodium*. Parasite proliferation within human red blood cells (RBC) is associated with the clinical manifestations of the disease. This asexual expansion within human RBCs, begins with the invasion of RBCs by *P. falciparum*, which is mediated by the secretion of effectors from two specialized club-shaped secretory organelles in merozoite-stage parasites known as rhoptries. We investigated the function of the Rhoptry Neck Protein 11 (RON11), which contains seven transmembrane domains and calcium-binding EF-hand domains. We generated conditional mutants of the *P. falciparum* RON11. Knockdown of RON11 inhibits parasite growth by preventing merozoite invasion. The loss of RON11 did not lead to any defects in processing of rhoptry proteins but instead led to a decrease in the amount of rhoptry proteins. We utilized ultrastructure expansion microscopy (U-ExM) to determine the effect of RON11 knockdown on rhoptry biogenesis. Surprisingly, in the absence of RON11, fully developed merozoites had only rhoptry each. The single rhoptry in RON11 deficient merozoites were morphologically typical with a bulb and a neck oriented into the apical polar ring. Moreover, rhoptry proteins are trafficked accurately to the single rhoptry in RON11 deficient parasites. These data show that in the absence of RON11, the first rhoptry is generated during schizogony but upon the start of cytokinesis, the second rhoptry never forms. Interestingly, these single-rhoptry merozoites were able to attach to host RBCs but are unable to invade RBCs. Instead, RON11 deficient merozoites continue to engage with RBC for prolonged periods eventually resulting in echinocytosis, a result of secreting the contents from the single rhoptry into the RBC. Together, our data show that RON11 triggers the *de novo* biogenesis of the second rhoptry and functions in RBC invasion.

INTRODUCTION

Malaria remains a devastating disease that affected approximately 249 million people worldwide in 2022, with the African region accounting for over 95% of the cases (World Health Organization 2023). The main causative agent of malaria is the unicellular protozoan parasite *Plasmodium falciparum*, which belongs to the apicomplexan phylum, along with other medically important organisms such as *Toxoplasma gondii* and *Cryptosporidium parvum*. Clinical symptoms of malaria in humans are associated with the continuous cycle of invasion of red blood cells (RBCs), development and replication within RBCs, and egress from RBCs to release new merozoites that perpetuate the cycle. Invasion is a process that has been targeted by multiple vaccination and antibody treatment strategies (Beeson et al. 2016; González-Sanz et al. 2023), which underscores the importance of understanding this process for the development of clinical interventions.

Invasion is a rapid and complex process involving multiple steps. Newly egressed merozoites initiate an early attachment, leading to RBC deformation and merozoite reorientation (Groomes et al. 2022; Hart et al. 2023; Weiss et al. 2015). Once its apical end is reoriented towards the RBC, the merozoite seems to form a pore in the RBC membrane, secretes proteins from rhoptries into the RBC, which together with micronemal proteins on the merozoite membrane, form an irreversible tight junction at the interface merozoite-RBC (Geoghegan et al. 2021; Riglar et al. 2011; Vulliez-Le Normand et al. 2012; Weiss et al. 2015). Subsequently, the merozoite utilizes its actinomyosin motor to push through the tight junction and internalize within the newly formed parasitophorous vacuole (PV) (Blake et al. 2020; Geoghegan et al. 2021; Perrin et al. 2018; Yahata et al. 2021). Within the PV, merozoites develop into their ring stage, progressing into their metabolically active forms, trophozoites, and finally into their replicative form, schizonts, which make 16-32 daughter merozoites. The parasite then initiates a cascade of events leading to the rupture of the RBC and PV membranes, resulting in the egress of merozoites (Dvorin and Goldberg 2022).

Rhoptries are two specialized secretory organelles localized to the apical end in apicomplexans known to be essential for parasite proliferation. Even though they carry conserved roles among apicomplexans, they vary in numbers according to species, for instance *Cryptosporidium spp*. have a single rhoptry, *Plasmodium spp*. have two in the asexual stages, and *Toxoplasma spp.* can have from eight to twelve rhoptries (Mageswaran et al. 2021; Martinez et al. 2022; Segev-Zarko et al. 2022). In *P. falciparum*, rhoptries are a pair of club-shaped secretory organelles located at the apical end of the merozoite that secrete proteins facilitating different steps during invasion. Rhoptries are internally compartmentalized into two regions: the neck and bulb, storing specific groups of proteins that are secreted at each step of invasion (Counihan et al. 2013; Liffner et al. 2021). Rhoptry neck proteins are assumed to be released first, primarily mediating attachment to RBCs and the formation of the tight junction through secretion of proteins from the RON complex (Srinivasan et al. 2011; Weiss et al. 2015). In contrast, rhoptry bulb proteins are secreted after tight junction formation and are associated with proper development within the PV, such as RAP1 and RAP2, which form the RAP complex (Ghosh et al. 2017; Riglar et al. 2011). During invasion, rhoptries fuse their necks and bulbs to form a single rhoptry (Hanssen et al. 2013). After invasion is completed, this single rhoptry is assumed to be disassembled, as rhoptries are absent during early ring stages. During schizogony, rhoptries are then formed *de novo* by the fusion of Golgi-derived vesicles (Bannister et al. 2000; Krai et al. 2014).

Rhoptry biogenesis begins early during schizogony, where the rhoptries remain associated with the cytoplasmic extensions of the outer centriolar plaque (CP) branches in a 1:1 ratio with each new rhoptry forming *de novo* through each remaining mitotic event, until the last event where this ratio is broken and each outer CP branch is observed with 2 rhoptries (Bannister et al. 2000; Liffner et al. 2023; Rudlaff et al. 2020). The final rhoptry pairs undergo *de novo* biogenesis instead of dividing from a common rhoptry precursor (Liffner et al. 2023), as it was previously assumed. Rhoptries maintain a bulb shape throughout most of their biogenesis process, adopting their final shape only after merozoite segmentation, with the formation of the neck in each rhoptry (Bannister et al. 2000; Liffner et al. 2023). Nevertheless, the molecular factors regulating rhoptry biogenesis, their structure, and internal compartmentalization are unknown.

Rhoptry neck protein 11, or RON11 (PF3D7_1463900), is a conserved, seven transmembrane domain protein with a pair of calcium-binding EF-hand domains at its C-terminus. Initial attempts to disrupt *P. berghei* RON11 were unsuccessful (Lasonder et al. 2008; van Ooij et al. 2008), while a recent knockdown showed a potential role in sporozoite invasion and gliding motility (Bantuchai et al. 2019). In contrast, RON11 disruption in *T. gondii* showed only a minor fitness defect, suggesting a non-essential role (Wang et al. 2016). However, nothing is known about the role of RON11 in *P. falciparum*. In this study, we employed the tetR-DOZI conditional knockdown system (Rajaram et al. 2020) to investigate the function of RON11 in the *P. falciparum* intraerythrocytic asexual life cycle. Our findings revealed that RON11 is essential for the intraerythrocytic growth of *P. falciparum.* Parasites lacking RON11 are unable to invade RBCs. Anti-RON11 antibodies are able to block merozoite invasion into RBCs suggesting that RON11 plays an essential role during invasion. Surprisingly, RON11 knockdown results in merozoites that have a single rhoptry. These single rhoptry merozoites are unable to complete invasion, even though they attach and secrete the contents from the single rhoptry into RBCs. Collectively, our data show that RON11 plays an essential role in regulating the *de novo* formation of the second rhoptry during merozoite segmentation and during merozoite invasion.

RESULTS

RON11 is essential for *P. falciparum* intraerythrocytic life cycle

To investigate the role of RON11 in *P. falciparum*, we generated RON11 conditional knockdown parasite lines employing the tetR-DOZI aptamer system, termed as RON11^{apt} (Rajaram et al. 2020). Using CRISPR/Cas9 technology, we integrated the tetR-DOZI system into the endogenous loci of RON11, leading to the expression of a hemagglutinin (HA)-tagged protein under the regulation of anhydrotetracycline (aTc) (Fig. 1A). PCR analysis of genomic DNA from RON11^{apt} parasites showed correct integration at the endogenous loci (Fig. 1B). To test the efficiency of the knockdown system, we evaluated protein expression both in the presence (+RON11) and absence (-RON11) of aTc via western blotting. Lysates from RON11^{apt} parasites cultured without aTc for 44 hours post-invasion (hpi) (from ring to schizont stages) exhibited around 97% of reduction in protein expression (Fig. 1C), confirming the system's suitability for studying RON11 function. Parasite growth was mearured using flow cytometry (Fig. 1D). These data show that RON11 is essential for parasite expansion, as -RON11 parasites failed to progress past their first life cycle (Fig. 1D).

Furthermore, we assessed the subcellular localization of RON11, which was previously observed in rhoptries of *P. berghei* schizonts (Bantuchai et al. 2019) (Fig. 1E). RON11 was localized with two well-known markers of the rhoptry neck (RON4) and rhoptry bulb (RAP1) (Fig. 1E). Our data showed the presence of RON11 in the rhoptry neck, as suggested by its colocalization with RON4 (Fig. 1E, top panels, and 1F). RON11 did not colocalize with RAP1, suggesting that RON11 is confined to the neck region (Fig. 1E, bottom panels, and 1F). Additionally, we observed RON11 at the parasite periphery of newly invaded ring-stage parasites (Supp. Fig. 1), suggesting that RON11 might localize to the parasitophorous vacuole (PV) after invasion, in a similar way to RAP1 (Anaguano et al. 2023; Liffner et al. 2023; Riglar et al. 2011). Taken together, these data show RON11 localizes to the rhoptry neck in schizonts, and in early-ring-stage parasites, it localizes at the parasite periphery.

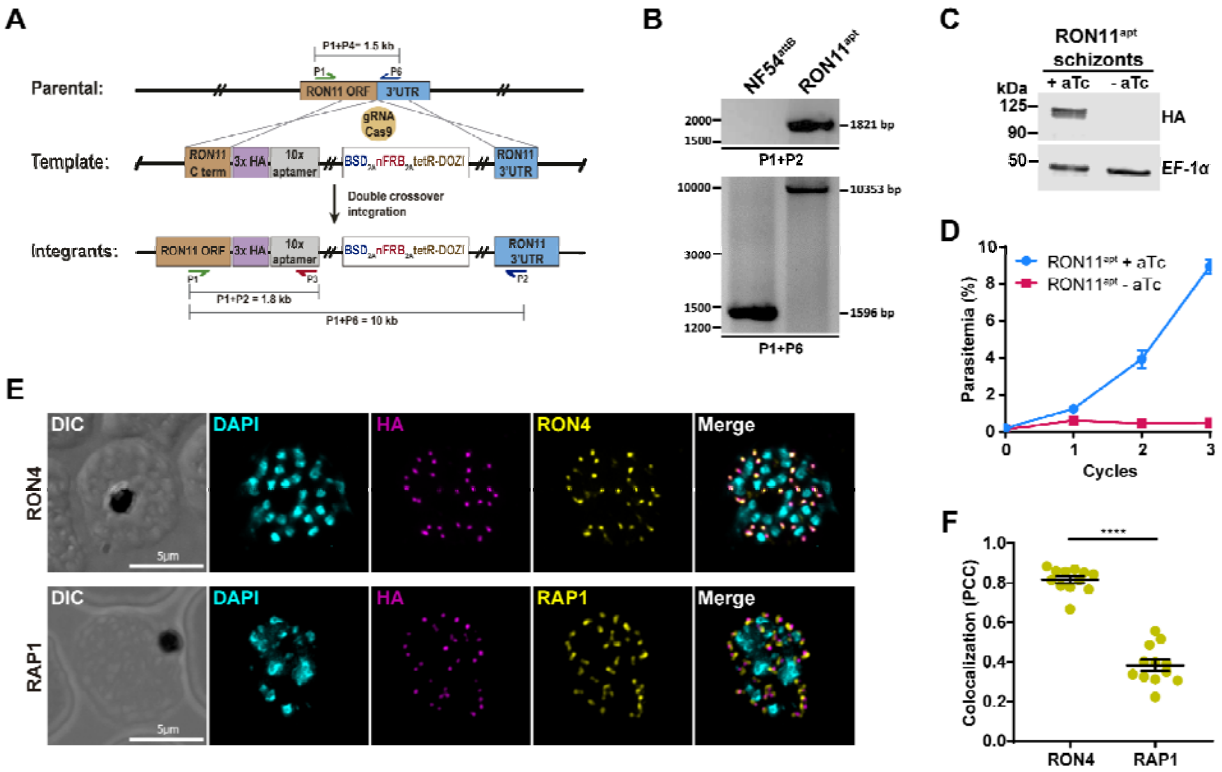

Figure 1. RON11 is essential for intraerythrocytic growth. (A) Schematic showing the integration of the repair plasmid used to introduce the tetR-DOZI system in the genomic loci of RON11. Cas9 introduces a double-stranded break at the C-terminus of the RON11 locus. The repair plasmid provides homology regions for double-crossover homologous recombination, introducing the system and providing a new 3'UTR to the gene. **(B)** PCR confirming integration at the RON11 locus. Amplicons were amplified from genomic DNA isolated from mutant and the parental line (NF54^{attB}) (Nkrumah et al. 2006). Primers were designed to amplify two regions: between the C-terminus and the 3'UTR of RON11, and between the C-terminus of RON11 and the new aptamer tandem. **(C)** Western blot of lysates from RON11^{apt} schizont grown in the presence and absence of 0.5 µM aTc. Lysates were probed with antibodies against HA (RON11) and EF1α (loading control). The protein marker sizes are shown on the left. (n = 4 biological replicates). **(D)** Growth of RON11^{apt} parasites over 3 intraerythrocytic life cycles in the presence and absence of 0.5 µM aTc. Synchronous parasites were collected every 48 hours, stained with the DNA dye Hoechst 33342, and measured via flow cytometry. One representative data set of three biological replicates shown. (n = 3 technical replicates; error bars = standard deviation (SD)). **(E)** IFAs showing the localization of RON11 in RON11^{apt} schizont with respect to two rhoptry markers: RON4 (neck) and RAP1 (bulb). Synchronous parasites were fixed with acetone and stained with specific antibodies. Images from left to right are phase-contrast, DAPI (nucleus, cyan), anti-HA (magenta), anti-RON4 or RAP1 (yellow), and fluorescence merge. Z stack images were deconvolved and projected as a combined single image. Representative images of 3 biological replicates. **(F)** Quantification of the colocalization of RON11^{apt} with

RON4 and RAP1 as determined by the Pearson's correlation coefficient (PCC). (n = 3 biological replicates, 4 schizonts per replicate. Error bars = standard error of the mean (SEM); ****p < 0.0001 by unpaired two-tailed t-test).

RON11 is required for merozoite invasion

As RON11 is known to be highly expressed in schizont stages (Bozdech et al. 2003; Llinás et al. 2006), and we showed its knockdown inhibits parasite growth (Fig. 1D), we sought to investigate whether RON11 is necessary for schizont development, egress or merozoite invasion. Therefore, we monitored the progression of synchronized RON11^{apt} parasites through their different life stages, both in the presence and absence of aTc. Samples were collected at all the stages, starting with tightly synchronized schizonts (46-48 hpi), using Hema3-stained smears and light microscopy. Our findings indicate that, both +RON11 and -RON11 parasites developed normally from rings through schizonts, and merozoites egressed at 48 hpi. (Fig. 2A). However, upon RON11 knockdown, the egressed merozoites did not produce rings, instead, they accumulated around the RBCs (Fig. 2A). To quantify our microscopy-based observations, we used flow cytometry to measure parasite development in egress-arrested schizonts. We confirmed that even though schizonts egressed in the absence of RON11, rings were not detected at any time point after egress (Fig. 2B). Together these findings suggest that the knockdown of RON11 prevents merozoite invasion, while having no effect on intracellular development or egress of merozoites.

The defect in invasion of -RON11 parasites could be either due to a deficiency in rhoptry biogenesis or due to a specific function of RON11 during RBC invasion. To differentiate between these two possibilities, we generated antibodies against the N-terminus of RON11 (aa32-442) (Sup. fig. 6A-B). As RON11 contains seven predicted transmembrane domains, prediction of protein orientation on the rhoptry membrane suggest that the N-terminus may face the rhoptry lumen. We hypothesized that this region may become accessible to antibodies during merozoite invasion when rhoptry contents are secreted. Western blot analysis detected a single high molecular weight

protein of the expected size in schizont lysate (Sup. fig. 6D). Widefield immunofluorescence microscopy using HA-tagged RON11 parasite line with anti-RON11 antibody detected the protein in puncta that overlapped with the HA and RAP1 (Sup. fig. 6E). We then evaluated the ability of anti-RON11 antibodies to block merozoite invasion and therefore reduce parasite multiplication. In these neutralization assays, parasites were incubated with anti-RON11 antibodies and their ability to proliferate was measured. *P. falciparum* parasites (3D7 strain) were incubated with various concentrations of total anti-RON11 IgG and parasite growth was measured by flow cytometry (Fig. 2C). Antibodies against RON11 exhibited concentration-dependent growth inhibitory activity, with around 80% growth inhibition at a concentration of 15 mg/mL (Fig. 2C). This suggests that the N-terminus of RON11 is accessible to antibodies during merozoite invasion and may interfere with its function in RBC invasion. Together with our RON11 conditional knockdown data, these findings support a putative role for RON11 in merozoite invasion.

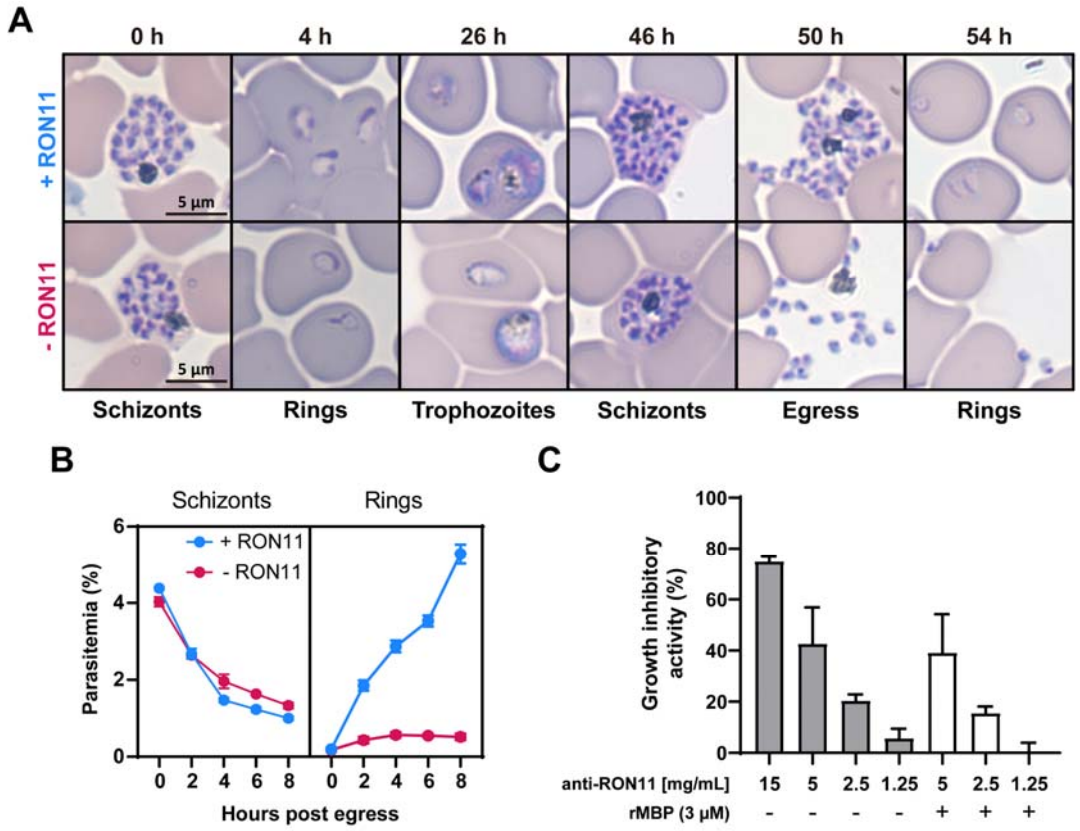

Figure 2. RON11 is required for merozoite invasion. (A) Representative Hema-3-stained blood-smears showing the development of RON11^{apt} parasites in the presence and absence of 0.5 μM aTc. Synchronous parasites were smeared, stained, and imaged at different time points by light microscopy. **(B)** Tracking of the development of synchronous RON11^{apt} parasites over 8 hours post-egress in the presence and absence of 0.5 μM aTc. Schizonts were tightly synchronized using 2 μM Compound 1. Synchronized parasites were collected every 2 hours, stained with Hoechst 33342, and measured via flow cytometry to distinguish between rings and schizonts. One representative data set of three biological replicates shown. (n = 3 technical replicates; error bars = SD). **(C)** *In vitro* neutralization assay was performed against 3D7 parasites using total IgG purified from rats immunized with rMBP-RON11 (N-term). Potential influence of anti-MBP antibodies was evaluated by pre-incubating IgG with rMBP(3μM). Parasites were stained with SYBR green and parasitemia was measured by flow cytometry. Growth inhibitory activity is represented as the percentage (%) of inhibition relative to the "no-IgG" control. (n = 2-4 biological replicates in duplicate; error bars = SEM).

RON11 is not required for merozoite attachment or eventual rhoptry discharge

Merozoite invasion is a complex multistep process, which involves the participation of multiple regulatory factors. In general terms, invasion can be divided into several discrete steps: attachment, apical end reorientation, RBC deformation, and pore formation, rhoptry secretion and tight junction formation, internalization and PVM sealing, and echinocytosis (Cowman et al. 2017; Groomes et al. 2022). To dissect the specific role of RON11 during merozoite invasion, we investigated the following specific events during invasion: attachment, deformation, rhoptry secretion and echinocytosis.

First, we used live-cell imaging to examine the merozoite-RBC interactions in recently egressed RON11^{apt} merozoites in the presence and absence of RON11 (Fig. 3A, Movie S1, and Movie S2). As shown previously (Fig. 2A and 2B), RON11 knockdown completely inhibited invasion in merozoites that induced deformation (n = 0/53), in contrast to the +RON11 merozoites in which 77.2% (n = 27/35) of merozoites invaded successfully (Fig. 3A). These invasion defects in -RON11 merozoites were observable even though these merozoites are capable of generating strong deformations of the RBC membrane (Fig. 3D) similar to +RON11 merozoites (p = 0.048). The -RON11 merozoites were capable of inducing echinocytosis (n = 33/44) in the attached RBCs (Fig 3C and Movie S2) . We also noticed that -RON11 merozoites continue to engage

with the RBCs (deformation) for longer periods of time and remain attached to RBCs, eventually leading to echinocytosis (Sup. Fig 2C). However, no significant difference between +RON11 and -RON11 merozoites was observed in the time that it took the merozoites from their initial contact with RBCs to the beginning of echinocytosis (Fig. 3E). Altogether, these data suggest that RON11 is not required for initial attachment, reorientation and deformation of RBCs, but is essential for internalization into the host cell. The longer deformation eventually leading to echinocytosis suggests secretion of contents from the single rhoptry into the RBC, albeit delayed.

To investigate defects in attachment of -RON11 parasites, we used a cytochalasin-D-based strategy to observe merozoite-RBC interactions (Riglar et al. 2011). Cytochalasin D is an actin polymerization inhibitor that disrupts the activity of the merozoite actomyosin motor, preventing internalization but not affecting the previous steps on merozoite invasion, such as attachment and rhoptry secretion (Boyle et al. 2010; Geoghegan et al. 2021; Riglar et al. 2011). Samples for analysis were collected from Compound 1 treated mature schizonts that were washed and allowed to invade fresh RBCs in the presence of cytochalasin D (Sup. fig. 2E).

First, we used light microscopy to observe +RON11 and -RON11 merozoites attached to RBCs. In merozoites incubated in cytochalasin D, no significant difference in the numbers of attached +RON11 or -RON11 merozoites was observed (Sup. fig. 2F). When merozoites were allowed to invade without cytochalasin D, we found more attached -RON11 merozoites, comparable to the cytochalasin-D-treated +RON11 merozoites (Sup. fig. 2G). As expected, the number of attached merozoites dropped significantly when cytochalasin D was removed from +RON11 merozoites, as they were able to invade RBCs and form rings (Sup. fig. 2G). Together, these data demonstrated that RON11 is not required for merozoite attachment to RBCs.

Next, we used IFAs to analyze the secretion of rhoptry proteins from cytochalasin-D-treated merozoites into RBCs in the +RON11 and -RON11 parasites. Live imaging data shows that echinocytosis occurs in -RON11 parasites (Fig. 3D and Sup. fig. 2B, 2C). Since echinocytosis is thought to be a result of rhoptry discharge into the RBC, these data suggest that -RON11 parasites are able to secrete rhoptry contents into the RBC.

To test this, we selected RAP1 as a rhoptry secretion marker because it has been previously shown to be secreted into RBCs cytoplasm in the presence of cytochalasin D (Riglar et al. 2011). We found that -RON11 merozoites were able to secrete RAP1 into RBCs similarly to +RON11 merozoites (Fig. 3F). Comparing the number of attached merozoites that secreted RAP1 into RBCs versus the ones who did not, no significant differences were observed between +RON11 and -RON11 parasites (Fig. 3G). These results, together with our observation of prolonged deformation prior to echinocytosis by live video microscopy, suggest that RON11 deficient merozoites are able to eventually secrete contents of their single rhoptry into the RBC.

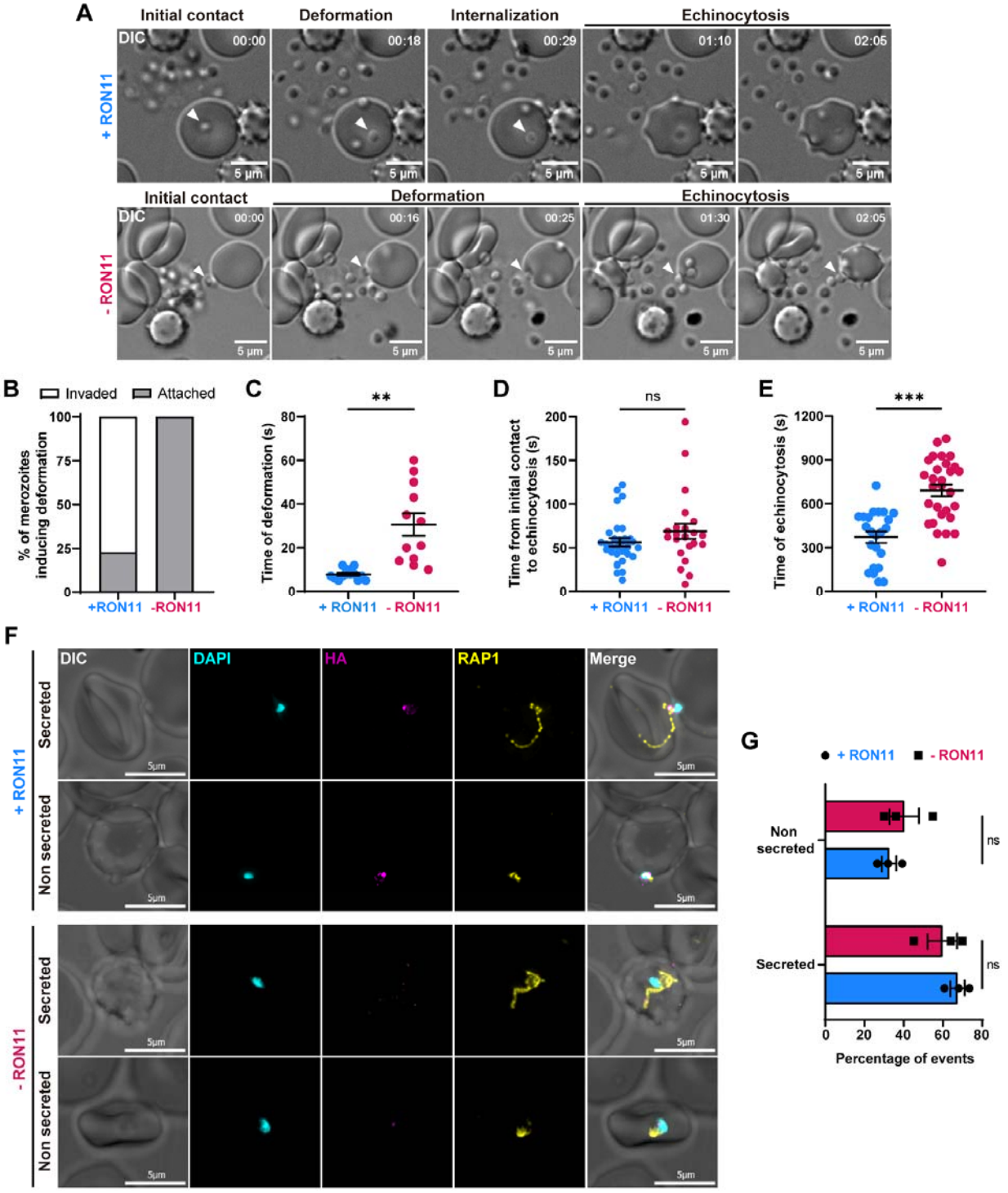

Figure 3. RON11 is not required for merozoite attachment nor rhoptry secretion. (A) Representative time-course images from Movie S1 (+RON11) and Movie S2 (-RON11) showing RON11^{apt} merozoites (arrowhead) interacting with RBCs in the presence and absence of 0.5 µM aTc. Images show the different stages of merozoite invasion post RBC initial contact. One representative data set of three biological replicates shown. **(B)** Quantification of merozoites that induced deformation in RBCs that

completed invasion or remained attached. (n = 3 biological replicates, 35 merozoites for +RON11 and 53 for -RON11). **(C)** Duration of merozoite-induced RBC deformation quantified using live video microscopy. (n = 3 biological replicates, 14 merozoites for +RON11 and 12 for -RON11; error bars = SEM; **p < 0.01 by unpaired two-tailed t-test). **(D)** Duration between merozoite first contact with RBCs and echinocytosis quantified using live video microscopy. (n = 3 biological replicates, 35 merozoites for +RON11 and 53 for -RON11; error bars = SEM; ns = non-significant by unpaired two-tailed t-test). **(E)** Duration of echinocytosis quantified using live video microscopy. (n = 3 biological replicates, 23 merozoites for +RON11 and 29 for -RON11; error bars = SEM; ***p < 0.001 by unpaired two-tailed t-test). **(F)** Representative IFAs showing RON11^{apt} attached-merozoites secreting RAP1 into RBCs in the presence or absence of aTc, after incubation with cytochalasin D. Parasites were fixed with PFA and stained with specific antibodies. Images from left to right are phase-contrast, DAPI (nucleus, blue), anti-HA (green), anti-RAP1 (red), and fluorescence merge. Z stack images were deconvolved and projected as a combined single image. Representative images of 3 biological replicates. **(G)** Quantification of RON11^{apt} attached-merozoites secreting RAP1 into RBCs. Slides were blinded and secretion events were scored and represented as the percentage of events per 50 attached merozoites (n = 3 biological replicates, 50 events per replicate. Error bars = SEM; ns = non-significant by unpaired two-tailed t-test).

RON11 knockdown results in merozoites with one rhoptry

Given previous observations that other rhoptry membrane-associated proteins, such as RAMA, play a role in rhoptry formation and transport of rhoptry protein (Sherling et al. 2019), we sought to determine whether RON11 shares a similar function. Therefore, to determine if RON11 functions in rhoptry biogenesis, we employed ultrastructural expansion microscopy (UExM) in combination with NHS-ester staining to observe rhoptry structures (Liffner et al. 2023). We analyzed tightly synchronized schizonts that were cultured in the presence or absence of aTc. ML10 is a highly specific inhibitor of the cGMP-dependent protein kinase (PKG) that arrests parasites prior to egress (Ressurreição et al. 2020), allowing for a tighter synchronization.

We observed fully formed rhoptries exhibiting their distinctive structures: a slender and elongated neck at the apex, connected to an apical ring, and a distal rotund bulb (Fig. 4A, top panels), as previously reported (Liffner et al. 2023). Strikingly, almost all -RON11 merozoites had only one rhoptry (Fig. 4A and 4B). These single rhoptries displayed no discernible structural alterations, as all three, the neck, the bulb, and apical

ring, were still present in the proper orientation positioned at the apical end of the merozoite (Fig. 4A, bottom panels). In rare cases, we observed -RON11 schizonts with several rhoptries amassed in regions that appeared to be located outside of merozoites (Sup. fig. 3A). Basal complexes were visible at their maximum contraction at the basal end of the analyzed merozoites (Liffner et al. 2023), suggesting that RON11 knockdown had no impact on merozoite segmentation, and confirming that the analyzed merozoites were fully developed (Fig. 4A and Sup. fig. 3A). To validate this finding, we quantified the number of merozoites per schizont and found that the absence of RON11 did not affect the total number of merozoites, even though the number of rhoptries was reduced by half (Sup. fig. 3B). To our knowledge, this marks the first observation of such a unique phenotype, single rhoptry merozoites (or changes in rhoptry numbers), in *Plasmodium spp.* parasites.

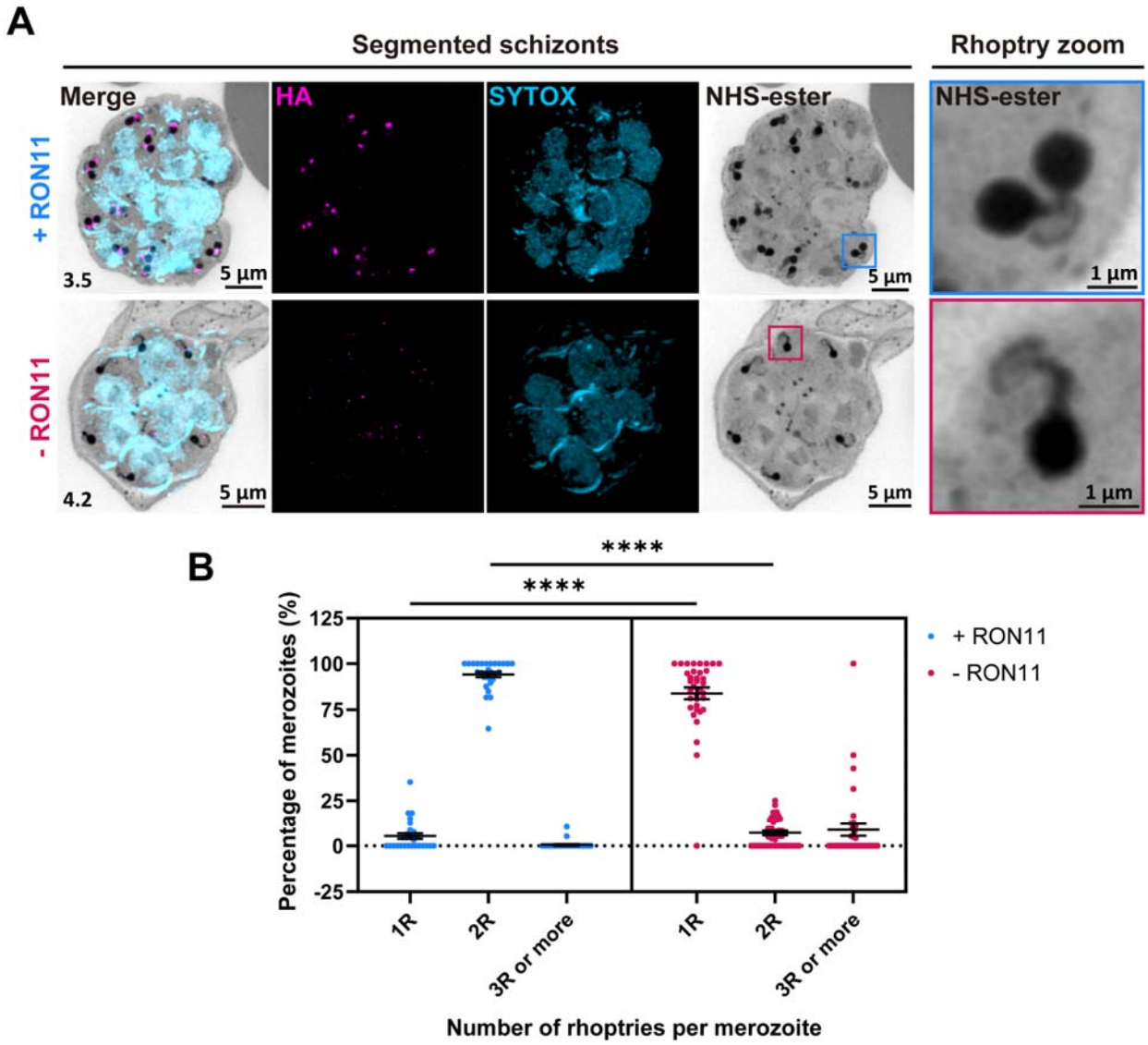

Figure 4. RON11 knockdown generates merozoites with single rhoptries. (A) Representative images of RON11^{apt} schizonts showing the structure of rhoptries within fully developed merozoites in the presence and absence of 0.5 µM aTc. ML10-arrested schizonts were expanded by U-ExM, fixed with PFA, and stained with NHS-Ester (greyscale), anti-HA (magenta), and the DNA dye SYTOX (cyan). Selected Z stack images were projected as a combined single image. Number on image = Z-axis thickness of projection in µm. **(B)** Quantification of merozoites with single, dual or multiple rhoptries in the presence and absence of 0.5 µM aTc. (n = 4 biological replicates, 28 schizonts for +RON11 and 36 for -RON11; error bars = SEM; ****$p < 0.0001$ by unpaired two-tailed *t*-test)

To further investigate the impact of RON11 knockdown on rhoptry structures, we analyzed the localization of other subcellular markers in segmented schizonts using UExM. We confirmed that RON11 localizes to the neck of fully formed rhoptries, along with its colocalization with RON4 (Fig. 4A, top panels, and 5A, top panels). Furthermore, the localization of RON4 and RAP1 remained unaltered in the single rhoptries in -RON11 parasites (Fig. 5A). Similarly, RON4 and RAP1 retained their localization in rhoptries of free -RON11 merozoites (Sup. fig. 4A).

Since -RON11 parasites had only one rhoptry, we wanted to test if the levels of rhoptry proteins were also decreased in these parasites. We assessed the expression of RON4 and RAP1 in fully matured +RON11 and -RON11 schizonts (48 hpi) using western blotting. The total amount of RON4 and RAP1 was reduced by approximately half in -RON11 parasites (Fig. 5B and 5C). This finding could be attributed to the reduction of the number of rhoptries by half, aligning with recent findings suggesting that rhoptry pairs form *de novo* during schizogony rather than through duplication from a single mother rhoptry (Liffner et al. 2023).

Finally, we evaluated the expression of markers of other subcellular compartments, such as the micronemes (AMA1) and merozoite surface (MSP1). We used IFAs and western blotting on fully mature E64-treated schizonts cultured in the absence of RON11. We observed no effect on protein content or secretion of MSP1 to the merozoite surface under RON11 knockdown (Sup. fig. 5A and 5B). Similarly, AMA1 retained its micronemal and secreted locations in the absence of RON11 (Sup. fig. 5C).

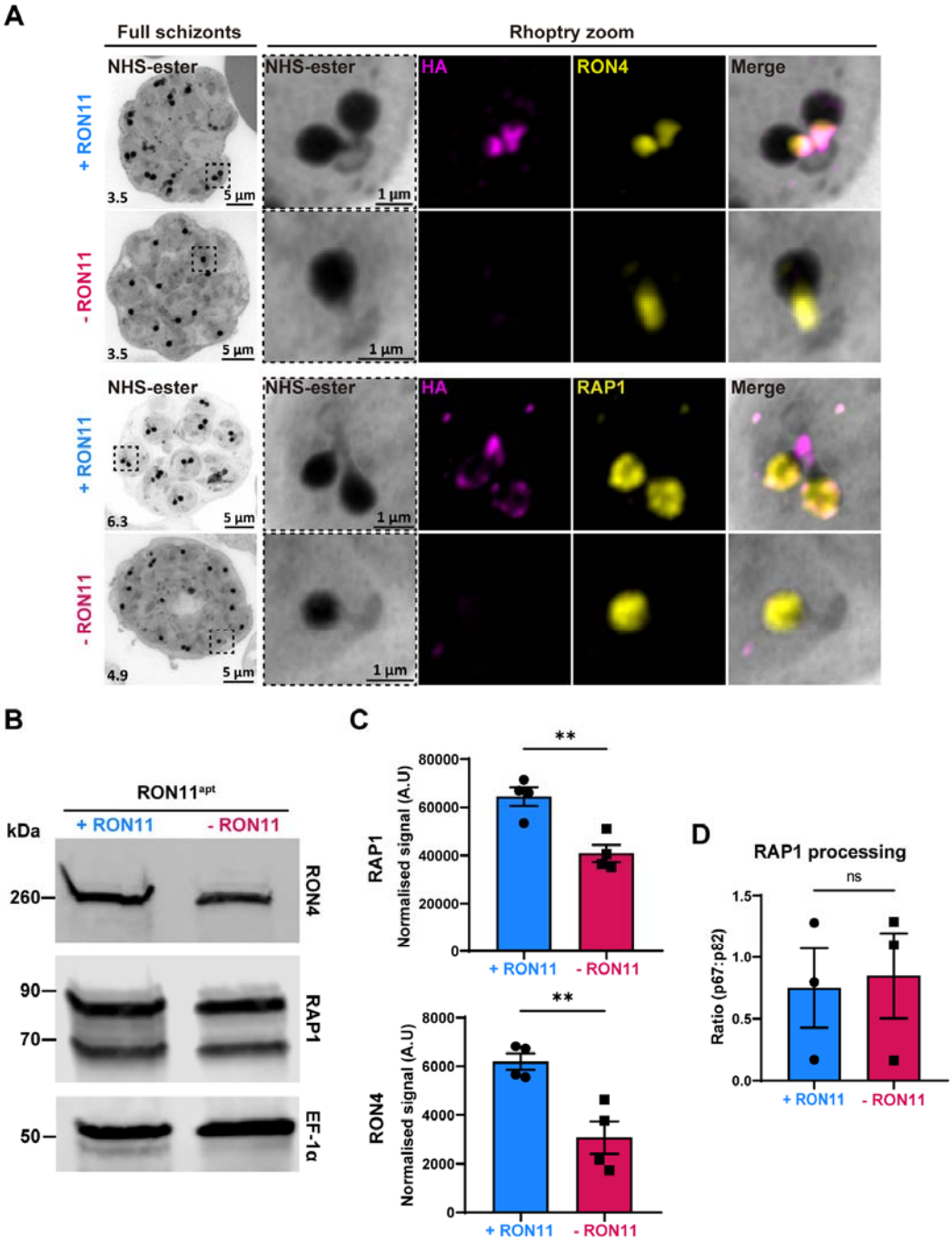

Figure 5. RON11 knockdown does not affect the localization and processing of neck and bulb rhoptry proteins. (A) Representative images of RON11^{apt} parasite showing the localization of RON11 with respect to RON4 and RAP1 in the presence and absence of aTc. E64-arrested parasites were expanded by U-ExM, fixed with PFA, and stained with NHS-Ester (greyscale), anti-HA (magenta), and RON4 or RAP1 (yellow). Selected Z stack images were projected as a combined single image. Number on image = Z-axis thickness of projection in µm. **(B)** Western blot of parasite lysates isolated from E64-

arrested RON11^{apt} parasites in the presence and absence of aTc. Samples were probed with antibodies against RON4, RAP1 and EF1α (loading control). The protein marker sizes are shown on the left. Representative blot of 4 biological replicates shown. **(C)** Quantification of the relative level of RON4 and RAP1 total protein content in E64-arrested RON11^{apt} parasites in the presence and absence of aTc. Band intensities were normalized to the loading control, EF1α, and are presented as normalized arbitrary units (A.U.) (n = 4 biological replicates; error bars = SEM; **p < 0.01 by unpaired two-tailed *t*-test). **(D)** Quantification of RAP1 processing in E64-arrested RON11^{apt} parasites in the presence and absence of aTc. Band intensities were normalized to the ratio of processed RAP1 (p67/p82) (n = 3 biological replicates; error bars = SEM; ns = non-significant by unpaired two-tailed *t*-test).

RON11 triggers the biogenesis of the last rhoptry pair

Rhoptries are first observed early during schizogony (Mahajan et al. 2008; Liffner et al. 2023) and our data shows that -RON11 merozoites have a single rhoptry. When does rhoptry biogenesis fail during schizogony and how does this generate single-rhoptry merozoites? Because schizogony is known to last approximately 15 hours (Voß et al. 2023), we designed a rescue assay to define the window of time within schizogony where restoring RON11 might restore parasite growth. Synchronized ring-stage RON11^{apt} parasites were grown with or without aTc and when these parasites reached schizogony (44 to 50 hpi), aTc was added back to the parasites at different time points (Fig. 5). The ability of these schizonts to form rings was measured using flow cytometry. Supplementation with aTc as late as 46 hpi restored the ability of -RON11 schizonts to generate ring stage parasites (Fig. 5). However, aTc supplementation after 46 hpi was unable to rescue growth (Fig. 5). These findings suggested that RON11 has an essential role during the final hours of schizont development.

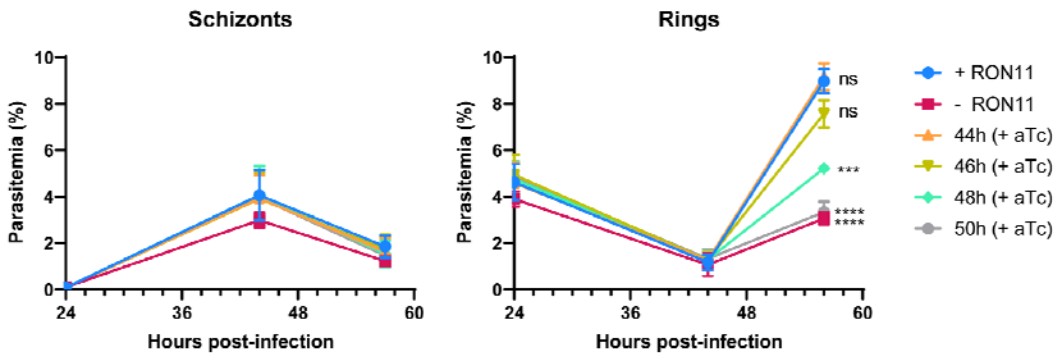

Figure 6. RON11 knockdown phenotype is rescued by addition of aTc during the last 2 hours of the asexual life cycle. Growth of RON11^{apt} parasites in the presence and absence of aTc. Tightly synchronous parasites were grown for 44 hpi and aTc was added back every two hours. Samples were collected at 24, 44 and 56 hpi, fixed in PFA, stained with the DNA dye Hoechst 33342, and measured via flow cytometry to differentiate between rings and schizonts. (n = 3 biological replicates; error bars = SEM; *ns = non-significant; ***p < 0.001; ****p < 0.0001 by one-way ANOVA compared to + RON11).

As we have shown that RON11 acts during the last hours of schizogony, we hypothesized it might have a role in regulating the formation of the last rhoptry pair during late schizogony. To test our hypothesis, we employed UExM in combination with NHS-ester to follow the development of rhoptry biogenesis during schizogony in the presence and absence of RON11. It has been previously shown that during their biogenesis, rhoptries associate with the branches of the outer CPs in a ratio of one rhoptry per branch during the early mitotic events of schizogony (Bannister et al. 2000; Liffner et al. 2023; Rudlaff et al. 2020). Once merozoite segmentation starts, each outer CP branch accommodates two rhoptries, which will form the final rhoptry pair within each merozoite (Liffner et al. 2023). By analyzing at 44-48 hour synchronized schizonts, we found that the formation and segregation of rhoptries during the mitotic events was not inhibited in -RON11 parasites (Fig. 7B and 7C). Surprisingly, we discovered that the loss of RON11 impaired the *de novo* formation of the second rhoptry after the last mitotic event (Fig. 7D). Initiation of merozoite segmentation on those events was confirmed by the presence of basal complex rings in association with the CP/rhoptry-complex densities (Fig. 7). Altogether this data confirms our thesis that RON11

regulates the *de novo* biogenesis of the second rhoptry after the last mitotic event during schizogony.

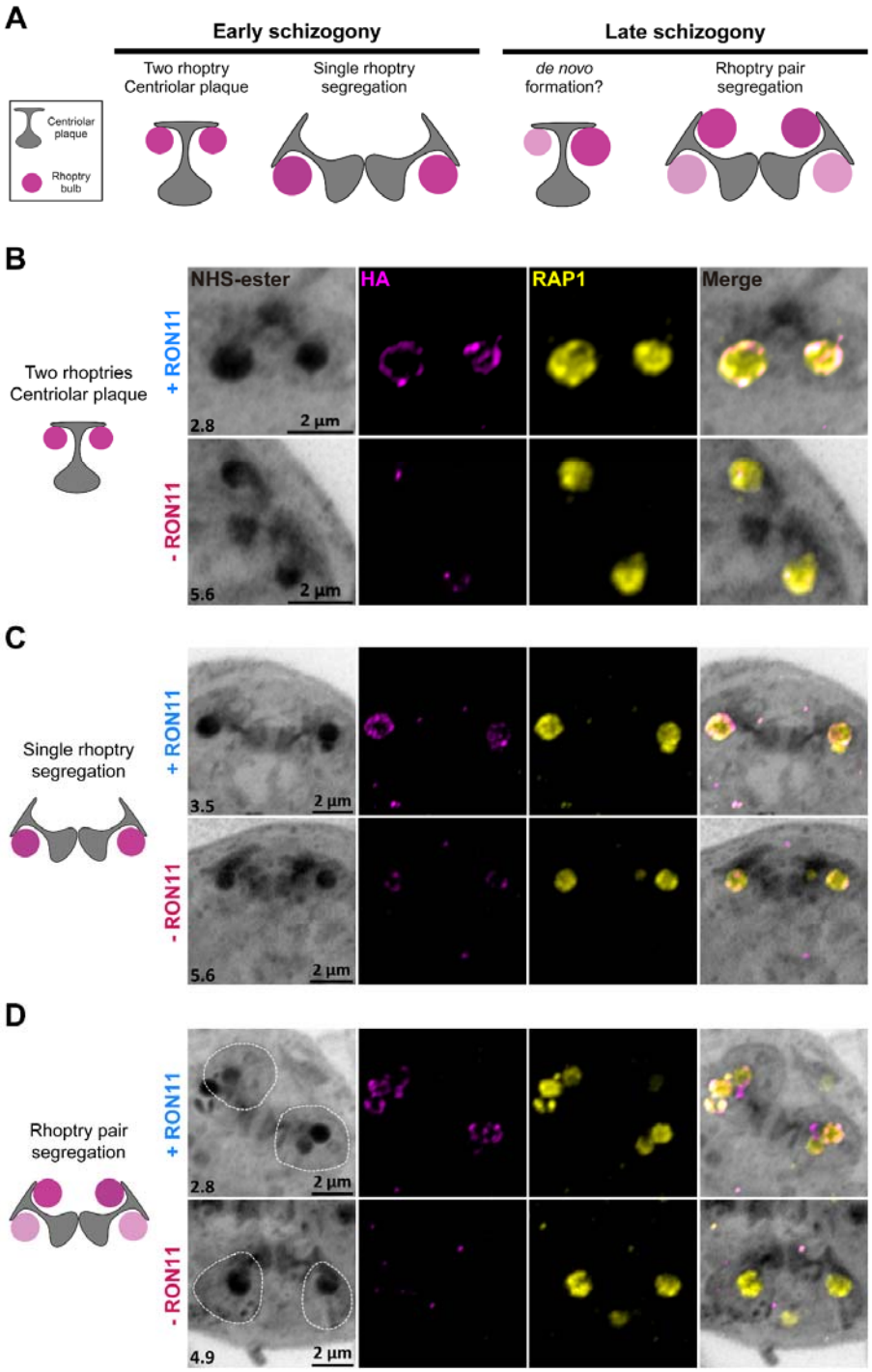

Figure 7. RON11 is required for the *de novo* biogenesis of the final rhoptry pair during merozoite segmentation. (A) Schematic of the current model for *de novo* formation of rhoptries during schizogony.

(B, C and D) Representative images of different steps of rhoptry biogenesis in RON11^{apt} late schizonts in the presence and absence of aTc: **(B)** Two rhoptries associated to each branch of a CP in the presence and absence of aTc, **(C)** Single rhoptries being segregated with each branch of a dividing CP during mitosis, and **(D)** Final rhoptry pairs being segregated with a CP branch during the final mitotic event. Basal complexes are demarcated by a discontinuous line. Late-schizont parasites were expanded by U-ExM, fixed with PFA, and stained with NHS-Ester (greyscale), anti-HA (magenta), and anti-RAP1 (yellow). Selected Z stack images were projected as a combined single image. Number on image = Z-axis thickness of projection in µm.

DISCUSSION

Similar to most rhoptry proteins studied to date in the asexual RBC stages (Liffner et al. 2021), we have demonstrated that RON11 is indispensable for parasite development, particularly merozoite invasion of RBCs. This aligns with previous failed attempts to generate RON11 knockouts in *P. berghei* parasites which supported essentiality of RON11 in blood stages (Lasonder et al. 2008; van Ooij et al. 2008). We used a combination of live cell video microscopy cytochalasin D- based attachment assays to show that initial engagement with RBC occurs normally in absence of RON11 but merozoites fail to enter into RBCs. While the actomyosin motor and its components are well-established as being involved in merozoite internalization (Blake et al. 2020; Perrin et al. 2018), no rhoptry protein has been associated with a role in this final stage of invasion. Interestingly, we observed by live imaging that RON11 knockdown merozoites that are unable to complete invasion, are still able to induce strong deformations on RBCs. Since gliding motility is required for deformation (Yahata et al. 2021; Hart et al. 2023), this suggests that RON11 may not be required for motility of *P. falciparum* merozoites, unlike previously observed for *P. berghei* sporozoites (Bantuchai et al. 2019). RON11 deficient merozoites engage and deform host cells for significantly longer duration before the RBCs undergo echinocytosis, a process that follows rhoptry secretion (Weiss et al. 2015). Therefore, RON11 may not be essential for rhoptry discharge but may affect the efficiency or timing of rhoptry secretion. In agreement with this observation RON11 knockdown merozoites in the presence of cytochalasin D proceeded to attach and secrete RAP1 into RBCs.

Following the kinetics of invasion by live cell microscopy also allows us to surmise the step of invasion where RON11 functions. Previous studies using this approach revealed key receptor-ligand interactions as molecular determinants of specific steps in merozoite invasion (Weiss et al. 2015). As -RON11 merozoites are able to attach, reorient and deform RBCs, it rules out a role for RON11 in these early steps. Following deformation, the RH5-basigin interaction leads to an opening at the interface of the merozoite and RBC initiating the secretion of rhoptry neck/bulb proteins. Blocking this interaction leads to normal deformation but prevents rhoptry secretion and no echinocytosis (Weiss et al. 2015). Finally, the AMA1-RON2 interaction mediates tight junction formation that provides an anchor and allows the actomyosin motor to drive the merozoite inside the RBC (Srinivasan et al. 2011). Peptide inhibitors of this interaction lead to strong deformation and echinocytosis, a result of rhoptry secretion (Weiss et al. 2015). Interestingly, RON11 knockdown resulted in merozoites unable to internalize but stay attached to the RBC and induce echinocytosis. This suggests that RON11 perhaps functions downstream of the RH5-basigin interaction. Furthermore, deformation times were significantly longer with RON11 knockdown merozoites compared to control merozoites (average of 21 sec and 6.5 sec respectively). Rhoptry secretion coincides with internalization and immediately follows the deformation step. The longer duration of deformation may therefore reflect a temporal defect in rhoptry secretion in the absence of RON11. These data are consistent with IFA data that show that RON11 is not required for the secretion of the rhoptry bulb protein, RAP1. However, since IFA uses fixed cells we cannot determine the kinetics of rhoptry secretion. Thus, it is possible that RON11 may play a role in ensuring timely secretion of rhoptry contents after the formation of the tight junction.

Calcium signaling plays a critical role during merozoite invasion. Following RBC deformation and immediately before internalization a prominent calcium signal is observed at the apical end of the invading merozoite, suggesting a potential role for calcium sensing protein(s) at this step of invasion (Weiss et al. 2015). This signal occurs downstream of RH5-basigin interaction and is not affected by AMA1-RON2 blocking peptide agonists (Weiss et al. 2015). It is possible that RON11 through its C-terminal EF

hand motifs may play a role in regulating the kinetics of rhoptry secretion and/or subsequent steps in invasion.

Rhoptries are critical secretory organelles conserved among apicomplexans, with differences in numbers depending on the species as well as between merozoite and sporozoite. During *P. falciparum* intraerythrocytic development, rhoptries are initially observed forming *de novo* during early schizogony (Liffner et al. 2023). Then, rhoptries replicate throughout multiple mitotic events until each merozoite contains two rhoptries by the end of the cycle. In contrast, *T. gondii* can have as many as 8-12 rhoptries, but only two are known to release their contents during invasion (Mageswaran et al. 2021). Rhoptry biogenesis remains a poorly understood process, primarily due to the small size of *P. falciparum*'s rhoptries, which, coupled with the limited resolution offered by conventional microscopy, has made their study challenging. Recent advances in microscopy techniques, such as UExM, have opened new possibilities for exploring these micron-sized secretory organelles (Liffner and Absalon 2023). Using UExM, we observed that RON11 is required for the proper biogenesis of rhoptry pairs, as its absence led to merozoites with single rhoptries, an unprecedented phenotype that has not been observed in any other apicomplexan system. Only three parasite proteins, Sortilin, RAMA and CERLI2, have been shown to have a role in the biogenesis of rhoptries in *P. falciparum* (Hallée et al. 2018; Liffner et al. 2022; Sherling et al. 2019). None of them share any structural similarities, localize to the same region within rhoptries, or generate a knockdown phenotype analogous to RON11. For instance, RAMA and CERLI2 loss causes morphological alterations in the rhoptry necks (Liffner et al. 2022; Sherling et al. 2019), while RON11's single rhoptries did not display any apparent structural change at the resolution of U-ExM imaging. Our data strongly suggests that RON11 is required for *de novo* rhoptry biogenesis at the end of schizogony, when daughter merozoites are being formed via cytokinesis. This thesis is supported by our initial observations by UExM that rhoptries are formed and segregated with the CPs without issues in -RON11 parasites during the asynchronous mitotic events of schizogony. These observations align with our findings that -RON11 parasite growth is rescued by reversing the knockdown as late as 46 hours post invasion, in the 48-hour asexual life cycle.

In contrast, we observed that the *de novo* formation of the initial rhoptry was not disrupted in -RON11 parasites during schizogony. However during cytokinesis, we noticed that one rhoptry was being distributed along with the dividing CPs into a nascent -RON11 merozoite, instead of two rhoptries as observed in +RON11 parasites. These observations are in agreement with our findings of a roughly 50% reduction in the number of rhoptries per schizont. Interestingly, we observed that RON11 knockdown also led to about a 50% reduction in the quantity of other rhoptry proteins, which is consistent with the finding that only half the amount of rhoptries are formed. This is a somewhat surprising result as prior work on other *P. falciparum* organelles suggest that a defect in organelle biogenesis does not lead to a loss in protein production. For example, upon loss of the parasite plastid known as the apicoplast, proteins targeted to the apicoplast are synthesized and appear to be stuck in secretory vesicles (Florentin et al. 2017; Florentin et al. 2020; Yeh and DeRisi 2011). Our data suggest that RON11 may function in a pathway that regulates synthesis of rhoptry proteins, either via transcription or translation. These data suggest that a signaling pathway may exist that ensures synthesis of rhoptry proteins only when rhoptry biogenesis occurs. Future transcriptomic and proteomic studies should resolve the role of RON11 in this *de novo* biogenesis pathway. Since RON11 has a pair of calcium binding EF-hand domains, it raises the possibility that a calcium-dependent pathway may function in biogenesis of rhoptries. During the final hours of schizogony, calcium-dependent pathways also trigger egress of the merozoites from the host RBC (Dvorin and Goldberg 2022). This study raises the possibility that a similar calcium signal may also kickstart, via RON11, the *de novo* biogenesis of the second rhoptry to ensure that the egressing merozoites have two rhoptries each for invading the next host RBC. It is unlikely that these are the same calcium signals because blocking the egress-specific calcium signal using PKG inhibitors does not prevent rhoptry biogenesis.

Together, these data suggest a model where RON11 has two functions in the final hours of the intraerythrocytic life cycle of *P. falciparum.* During segmentation of the schizont, RON11 is required to trigger the *de novo* biogenesis of the final rhoptry pair, which ensures each merozoite ends up with two rhoptries. After the merozoite makes contact with a new host RBC, RON11 is required for internalization into the new host

cell. Calcium signals play a critical role in both merozoite egress as well as invasion. It remains to be seen if the calcium binding EF-hand domains of RON11 play a role in either its function in rhoptry biogenesis or its function in merozoite invasion. The discovery of the biological function of RON11 now provides an avenue to investigate the molecular mechanisms driving rhoptry biogenesis and how it is linked to merozoite invasion.

MATERIALS AND METHODS

Construction of RON11 plasmids

Genomic DNA was isolated from *P. falciparum* NF54^{attB} cultures using the QIAamp DNA blood kit (Qiagen). PCR products were inserted into the respective plasmids using the NEBuilder HiFi DNA Assembly system (NEB). All constructs used in this study were confirmed by sequencing. All primers used in this study are in Table 3.1.

For generation of the plasmid pKD-RON11-Apt, sequences of approximately 500 bp of homology to the RON11 (Pf3D7_1463900) C-terminus and 3'UTR were amplified using primer pairs P3-P4 and P5-P6, respectively (Table 3.1). Amplicons were then inserted into pKD (Rajaram et al. 2020) digested by with AatII and AscI. For expression of a RON11 gRNA, oligo P7 was inserted into cut pUF1-Cas9 (Table 3.1).

Parasite culture and transfections

Plasmodium parasites were cultured in RPMI 1640 medium (NF54^{attB}, RON11^{apt}) supplemented with AlbuMAX I (Gibco), and transfected as described earlier (Kudyba et al. 2018).

For generation of RON11^{Apt} parasites, a mix of two plasmids (50 µg each) were transfected into NF54^{attB} parasites in duplicate. The plasmid mix contained the plasmid pUF1-Cas9-SBP1gRNA, which contains the DHOD resistance gene, and the marker-free plasmid pTOPO-SBP1-TbID. Drug pressure was applied 48 h after transfection,

using 1µM DSM1 (Ganesan et al. 2011) and selecting for Cas9 expression. After parasites grew back from transfection, integration was confirmed by PCR, and then cloned using limiting dilution. After clonal selection, cultures were transferred to biotin-free medium without DSM1.

For generation of RON11^{apt} parasites, the pKD-RON11-Apt plasmid (20 µg) and the respective pUF1-Cas9 plasmid (50 µg) were transfected into NF54^{attB} parasites in duplicate. Before transfection pKD plasmids were digested overnight with EcoRV (NEB). The enzyme was then subjected to heat inactivation for 20 min at 65 °C and then mixed with the pUF1-Cas9 plasmid. Transfected parasites were grown in 0.5 µM anhydrous tetracycline (aTc) (Cayman Chemical). Drug pressure was applied 48 h after transfection, using blasticidin (BSD) (Gibco) at a concentration of 2.5 µg/mL, selecting for pKD-RON11-Apt expression. After parasites grew back from transfection, integration was confirmed by PCR, and then cloned using limiting dilution. Clones were maintained in mediums containing 0.5 µM aTc and 2.5 µg/mL BSD.

Growth assays

For all assays, aliquots of parasite cultures were incubated in 8 µM Hoechst 33342 (ThermoFisher Scientific) for 20 min at room temperature and then fluorescence was measured using a CytoFlex S (Beckman Coulter) flow-cytometer. Flow cytometry data were analyzed using FlowJo software (Tree Star, Inc.) and plotted using Prism (GraphPad Software Inc.).

For the growth assay, synchronous ring-stage parasites were washed five times with RPMI 1640 medium and split into two cultures, one resuspended in medium containing 0.5 µM aTc and 2.5 µg/mL BSD (+RON11), and the other one in medium containing only 2.5 µg/mL BSD (-RON11). Cultures were then transferred to a 96-well plate at 0.2% parasitemia and grown for 6 days. Parasitemia was monitored every 48 h.

For the invasion vs egress assay, synchronous ring-stage parasites were washed and split into two cultures with and without aTc, as previously described. Parasites were then allowed to develop into mature schizonts to be isolated using a Percoll gradient

(Genesee Scientific). Enriched parasites were then incubated for 4 hours at 37 °C in pre-warmed RPMI media supplemented with the PKG inhibitor, ML10 compound (25 nM) (obtained from S. Osborne, BEI resources) (Ressurreição et al. 2020). After incubation, parasites were washed twice with pre-warmed RPMI media and transferred immediately to pre-warmed RBCs at 2% hematocrit. Parasitemia was monitored every two hours, for eight hours.

For the rescue assay, parasites were synchronized to a 1-hour window. Synchronized ring-stage parasites were washed and split into six cultures in a 6-well plate (+ RON11, - RON11, 44h, 46h, 48h and 50h). Culture "+RON11" was grown in the presence of aTc, while the others were grown in absence of aTc. Parasites were allowed to develop into schizonts and aTc was supplemented back into cultures at their corresponding time point, except for the "-RON11" culture. Parasitemia was monitored at 44 and 56 hours post infection (hpi).

Western blotting

Parasites were synchronized, washed, and split into two cultures with and without aTc, as previously described. Synchronous parasites were then allowed to develop into mature schizonts to be then incubated with E64 for 4 hours at 37 °C. After treatment, culture pellets were treated with ice-cold 0.04% saponin in 1x PBS to isolate parasites from host cells. The parasite pellets were subsequently solubilized in protein loading dye with Beta-mercaptoethanol (LI-COR Biosciences) and used for SDS-PAGE.

Primary antibodies used in this study included mouse-anti-HA (6E2; Cell Signaling Technology; 1:2000), rabbit-anti-PfEF1α (from Daniel Goldberg, 1:2000), mouse-anti-RAP1 (2.29; from Jana McBride via the European Malaria Reagent Repository; 1:500) (Hall et al. 1983), mouse-anti-RON4 (10H11; from Alan Cowman; 1:500) (Richard et al. 2010), mouse-anti-MSP1 (12.4; from Jana McBride via the European Malaria Reagent Repository; 1:500) (McBride, Newbold, and Anand 1985). Secondary antibodies used were IRDye 680 CW goat-anti-rabbit IgG and IRDye 800CW goat-anti-mouse IgG (Li-COR Biosciences; 1:20 000). Membranes were imaged using the Odyssey Clx Li-COR

infrared imaging system (Li-COR Biosciences). Images were processed and analyzed using ImageStudio (Li-COR Biosciences).

Microscopy and image analysis

For all microscopy assays, parasites were synchronized, washed, and split into two cultures with and without aTc, as previously described.

For IFAs, cells were fixed following the previously described protocol (Cobb et al. 2017).

For localization assays, schizont-stage parasites were smeared onto a slide, fixed and permeabilized with acetone for 10 min at room temperature.

For rhoptry secretion assays, synchronous parasites were allowed to develop into mature schizonts to be isolated using a Percoll gradient (Genesee Scientific). Enriched parasites were then incubated for 4 hours at 37 °C in pre-warmed RPMI media supplemented with 25 nM ML10 compound. After incubation, parasites were washed twice with pre-warmed RPMI media and transferred immediately to RBCs at 1% hematocrit. Cultures were then allowed to egress for 30 min at 37 °C in media supplemented with 1 µM cytochalasin D (Invitrogen). After incubation, parasites were fixed with 4% paraformaldehyde (PFA) (Electron Microscopy Sciences) and 0.03% glutaraldehyde, before being permeabilized with 0.1% Triton-X100.

Primary antibodies used in the IFAs included rabbit-anti-HA (SG77; ThermoFisher Scientific; 1:100), mouse-anti-RAP1 (2.29; from Jana McBride via the European Malaria Reagent Repository; 1:500) (Hall et al. 1983), mouse-anti-RON4 (10H11; from Alan Cowman; 1:200) (Richard et al. 2010). Secondary antibodies used were Alexa Fluor 488 and Alexa Fluor 546 (Life Technologies, 1:1000).

After mounting the cells using ProLong Diamond with 4’,6’-diamidino-2-phenylindole (DAPI) (Invitrogen), they were imaged using a DeltaVision II microscope system with an Olympus Ix-71 inverted microscope. Images were collected as a Z-stack and deconvolved using SoftWorx (GE HealthCare), then displayed as a maximum intensity projection. Adjustments to brightness and contrast were made for display purposes

using Adobe Photoshop. Colocalization was analyzed using the Pearson's correlation coefficient calculated by the Cell Profiler software (Broad Institute Inc.).

For growth assays, synchronous schizont-stage parasites were washed five times and split into two cultures, one without and one with aTc. Parasites were allowed to develop during two life cycles and sample aliquots were collected at different time points.

For attachment assays, parasites were collected as previously described in the rhoptry secretion assay with a slight change. After ML10 removal, schizont-stage parasites were allowed to egress during 2 h at 37 °C in the presence and absence of 1 µM cytochalasin D. Samples were collected after incubation.

For light microscopy imaging, aliquots were smeared into glass slides and stained using Hema3 Fixative solutions (Fischer Healthcare). Slides were imaged using a Zeiss Axio Scope A1 microscope with a Zeiss Axiocam 305 color camera. Images were processed using Adobe Photoshop.

Ultrastructural expansion microscopy (U-ExM)

Cultures for U-ExM were synchronized to mature schizont parasites, following the previously described methods. Ultrastructure expansion microscopy (U-ExM) was performed as described previously (Liffner and Absalon 2021), with minor modifications.

To start, 12 mm round coverslips were treated with poly-D-lysine for 1 hour at 37 °C. They were then washed three times with MilliQ water and placed in a 24-well plate. Parasite cultures with approximately 5% parasitemia were adjusted to 0.5% hematocrit. Then, 1 mL of parasite culture was added to the well containing the treated coverslip and incubated for 1 h at 37 °C.

After the incubation, the supernatant was carefully removed, and a fixative solution (4% v/v PFA in PBS) was added, followed by a 20 min incubation at 37 °C. The coverslips were washed three times with 1X PBS and incubated overnight at 37 °C in 500 µL of 1.4% formaldehyde/2% acrylamide (FA/AA) in PBS.

The monomer solution (19% sodium acrylate, 10% acrylamide, 0.1% N,N'-methylenebisacrylamide in PBS) was prepared a day prior and stored at -20 °C. Before gelation, coverslips were removed from FA/AA solution and washed three times in 1X PBS.

For gelation, 5 µL of 10% tetramethylenediamine (TEMED) and 5 µL of 10% ammonium persulfate (APS) were added to 90 µL of the monomer solution, briefly vortexed, and 35 µL of the monomer mixture were pipetted onto parafilm. The coverslips were placed on top with the cell-side facing down, and the gels were incubated at 37 °C for 30 min.

Next, the gels were transferred into a 6-well plate containing denaturing buffer (200 mM sodium dodecyl sulfate (SDS), 200 mM NaCl, 50 mM Tris, pH 9) and incubated for 15 min incubation at room temperature. Afterward, the gels were separated from the coverslips and transferred to 1.5 mL tubes with the denaturing buffer for 90-min incubation at 95 °C.

Subsequently, the gels were incubated with secondary antibodies diluted in 1X PBS for 2.5 hours. After denaturation, gels were transferred to Petri dishes containing 25 mL of MilliQ water and incubated three times for 30 min at room temperature with shaking, changing the water in between. The gels were measured and subsequently shrunk using two washes with 1X PBS. They were then transferred to a 24-well plate for blocking in 3% BSA in PBS at room temperature for 30 min. After blocking gels were incubated with primary antibodies diluted in 3% BSA overnight at room temperature.

Following primary antibody incubation, the gels were washed three times in 0.5% PBS-Tween 20 for 10 min before incubation with secondary antibodies diluted in 1X PBS for 2.5 hours.

After secondary antibody staining, the gels were washed three times with 0.5% PBS-Tween 20. Then, gels were transferred back to 10 cm Petri dishes for the second round of expansion, involving three incubations with MilliQ water. After re-expansion, the gels were either imaged immediately or stored in 0.2% propyl gallate in water until imaging.

The primary antibodies used were rat-anti-HA 3F10 (Roche, 1:25), mouse-anti-RAP1 (2.29; from Jana McBride via the European Malaria Reagent Repository; 1:500) (Hall et al. 1983), mouse-anti-RON4 (10H11; from Alan Cowman; 1:200) (Richard et al. 2010). The secondary antibodies used were Alexa Fluor 488 and Alexa Fluor 546 (Life Technologies, 1:500), NHS-ester 405 (Thermofisher, 1:250). The gels were imaged using a Zeiss LSM 980 microscope with Airyscan 2. Images were collected as a Z-stack, processed by Airyscan, and then displayed as a maximum intensity projection. Adjustments to brightness and contrast were made using ZEN Blue software for display purposes.

Expression and purification of recombinant RON11

A *E.coli* codon optimized DNA fragment corresponding to amino acids 32-442 of RON11 was synthesized (Genscript) and cloned into pMAL vector (NEB) in frame with an N-terminal maltose binding protein (MBP) tag and c-terminal His6 tag. Protein expression was induced using 0.4mM IPTG at 16°C for 12-14h. The cell pellet was resuspended in a lysis buffer (300mM NaCl, 10mM imidazole, 500mM NaH2PO4 and 1µM PMSF, 10mM BME, and 0.1% Tween20). Following sonication, the soluble fraction containing recombinant MBP-RON11-His6 protein was affinity purified twice on immobilized-metal affinity chromatography (IMAC) column using FPLC (Biorad) and further purified on CHT Ceramic Hydroxyapatite column. Fractions containing rMBP-RON11 were pooled and dialyzed into phosphate buffered saline (PBS) containing 1µM PMSF, 10mM BME and 0.1% Tween20 and kept at -80°C.

Animal immunization, IgG purification and neutralization assay

Animal experiments were approved by the Johns Hopkins Animal Care and Use Committee (ACUC, protocol# RA22H291). Four female Sprague Dawley rats (Charles River Laboratory), 5-6 weeks old, were used for immunizations. Recombinant MBP-RON11 (25µg/rat/immunization) was mixed 1:1 with Addavax adjuvant and injected subcutaneously three times in two-week intervals. Two weeks following the last immunization blood was collected by terminal heart bleed. Total rat IgG was purified

from serum using pre-equilibrated protein G column (GE health sciences), dialyzed against RPMI 1640 medium, and sterile filtered.

Synchronized trophozoite stage 3D7 strain parasites were adjusted to 0.5% parasitemia in 4% hematocrit in a 96-well plate and incubated with anti-RON11 IgG at the indicated concentrations with or without pre-incubation with 3µM rMBP protein. After 72 hours incubation at 37°C, cells were stained with SYBR Green I and parasitemia was measured using AttuneNxT flow cytometer (ThermoScientific).

ACKNOWLEDGEMENTS

We thank Dan Goldberg for anti-EF1α, Alan Cowman for anti-RON4, The European Malaria Reagent Repository for anti-RAP1 antibodies; Julie Nelson and Juan Bustamante at the CTEGD Cytometry Shared Resource Laboratory for help with flow cytometry and analysis; and Muthugapatti Kandasamy at the Biomedical Microscopy Core at the University of Georgia for help with microscopy. The study was funded by NIH/NIAID R56 AI73133 (V.M.), T32 AI060546 (G.S.V), T32 AI138953 (S.Y.), Office of the Vice-President for Research at UGA (D.A.), the CTEGD TIPS Fellowship and Daniel G. Colley Training in Parasitology Fund (D.A.), Johns Hopkins Malaria Research Institute predoctoral fellowship (O.A-F), and in part by the Johns Hopkins Malaria Research Institute and the Bloomberg Philanthropies (P.S.).

REFERENCES

Anaguano, David, Watcharatip Dedkhad, Carrie F. Brooks, David W. Cobb, and Vasant Muralidharan. 2023. “Time-Resolved Proximity Biotinylation Implicates a Porin Protein in Export of Transmembrane Malaria Parasite Effectors.” *Journal of Cell Science*, September. https://doi.org/10.1242/jcs.260506.

Bannister, L. H., J. M. Hopkins, R. E. Fowler, S. Krishna, and G. H. Mitchell. 2000.

"Ultrastructure of Rhoptry Development in Plasmodium Falciparum Erythrocytic Schizonts." *Parasitology* 121 (Pt 3) (September): 273–87.

Bantuchai, Sirasate, Mamoru Nozaki, Amporn Thongkukiatkul, Natcha Lorsuwannarat, Mayumi Tachibana, Minami Baba, Kazuhiro Matsuoka, Takafumi Tsuboi, Motomi Torii, and Tomoko Ishino. 2019. "Rhoptry Neck Protein 11 Has Crucial Roles during Malaria Parasite Sporozoite Invasion of Salivary Glands and Hepatocytes." *International Journal for Parasitology* 49 (9): 725–35.

Beeson, James G., Damien R. Drew, Michelle J. Boyle, Gaoqian Feng, Freya J. I. Fowkes, and Jack S. Richards. 2016. "Merozoite Surface Proteins in Red Blood Cell Invasion, Immunity and Vaccines against Malaria." *FEMS Microbiology Reviews* 40 (3): 343–72.

Blake, Thomas C. A., Silvia Haase, and Jake Baum. 2020. "Actomyosin Forces and the Energetics of Red Blood Cell Invasion by the Malaria Parasite Plasmodium Falciparum." *PLoS Pathogens* 16 (10): e1009007.

Bozdech, Zbynek, Manuel Llinás, Brian Lee Pulliam, Edith D. Wong, Jingchun Zhu, and Joseph L. DeRisi. 2003. "The Transcriptome of the Intraerythrocytic Developmental Cycle of Plasmodium Falciparum." *PLoS Biology* 1 (1): E5.

Charnaud, Sarah C., Rasika Kumarasingha, Hayley E. Bullen, Brendan S. Crabb, and Paul R. Gilson. 2018. "Knockdown of the Translocon Protein EXP2 in Plasmodium Falciparum Reduces Growth and Protein Export." *PloS One* 13 (11): e0204785.

Counihan, Natalie A., Ming Kalanon, Ross L. Coppel, and Tania F. de Koning-Ward. 2013. "Plasmodium Rhoptry Proteins: Why Order Is Important." *Trends in Parasitology* 29 (5): 228–36.

Cowman, Alan F., Christopher J. Tonkin, Wai-Hong Tham, and Manoj T. Duraisingh. 2017. "The Molecular Basis of Erythrocyte Invasion by Malaria Parasites." *Cell Host & Microbe* 22 (2): 232–45.

Ganesan, Suresh M., Joanne M. Morrisey, Hangjun Ke, Heather J. Painter, Kamal Laroiya, Margaret A. Phillips, Pradipsinh K. Rathod, Michael W. Mather, and Akhil B. Vaidya. 2011. “Yeast Dihydroorotate Dehydrogenase as a New Selectable Marker for Plasmodium Falciparum Transfection.” *Molecular and Biochemical Parasitology* 177 (1): 29–34.

Garten, Matthias, Armiyaw S. Nasamu, Jacquin C. Niles, Joshua Zimmerberg, Daniel E. Goldberg, and Josh R. Beck. 2018. “EXP2 Is a Nutrient-Permeable Channel in the Vacuolar Membrane of Plasmodium and Is Essential for Protein Export via PTEX.” *Nature Microbiology* 3 (10): 1090–98.

Geoghegan, Niall D., Cindy Evelyn, Lachlan W. Whitehead, Michal Pasternak, Phoebe McDonald, Tony Triglia, Danushka S. Marapana, et al. 2021. “4D Analysis of Malaria Parasite Invasion Offers Insights into Erythrocyte Membrane Remodeling and Parasitophorous Vacuole Formation.” *Nature Communications* 12 (1): 1–16.

Ghosh, Sreejoyee, Kit Kennedy, Paul Sanders, Kathryn Matthews, Stuart A. Ralph, Natalie A. Counihan, and Tania F. de Koning-Ward. 2017. “The Plasmodium Rhoptry Associated Protein Complex Is Important for Parasitophorous Vacuole Membrane Structure and Intraerythrocytic Parasite Growth.” *Cellular Microbiology* 19 (8). https://doi.org/10.1111/cmi.12733.

González-Sanz, Marta, Pedro Berzosa, and Francesca F. Norman. 2023. “Updates on Malaria Epidemiology and Prevention Strategies.” *Current Infectious Disease Reports*, June, 1–9.

Groomes, Patrice V., Usheer Kanjee, and Manoj T. Duraisingh. 2022. “RBC Membrane Biomechanics and Plasmodium Falciparum Invasion: Probing beyond Ligand-Receptor Interactions.” *Trends in Parasitology* 38 (4): 302–15.

Hallée, Stéphanie, Natalie A. Counihan, Kathryn Matthews, Tania F. de Koning-Ward, and Dave Richard. 2018. “The Malaria Parasite Plasmodium Falciparum Sortilin Is Essential for Merozoite Formation and Apical Complex Biogenesis.” *Cellular Microbiology* 20 (8): e12844.

Hanssen, Eric, Chaitali Dekiwadia, David T. Riglar, Melanie Rug, Leandro Lemgruber, Alan F. Cowman, Marek Cyrklaff, et al. 2013. “Electron Tomography of Plasmodium Falciparum Merozoites Reveals Core Cellular Events That Underpin Erythrocyte Invasion.” *Cellular Microbiology* 15 (9): 1457–72.

Hart, Melissa N., Franziska Mohring, Sophia M. DonVito, James A. Thomas, Nicole Muller-Sienerth, Gavin J. Wright, Ellen Knuepfer, Helen R. Saibil, and Robert W. Moon. 2023. “Sequential Roles for Red Blood Cell Binding Proteins Enable Phased Commitment to Invasion for Malaria Parasites.” *Nature Communications* 14 (1): 4619.

Krai, Priscilla, Seema Dalal, and Michael Klemba. 2014. “Evidence for a Golgi-to-Endosome Protein Sorting Pathway in Plasmodium Falciparum.” *PloS One* 9 (2): e89771.

Kudyba, Heather M., David W. Cobb, Anat Florentin, Michelle Krakowiak, and Vasant Muralidharan. 2018. “CRISPR/Cas9 Gene Editing to Make Conditional Mutants of Human Malaria Parasite P. Falciparum.” *Journal of Visualized Experiments: JoVE*, no. 139 (September). https://doi.org/10.3791/57747.

Lasonder, Edwin, Chris J. Janse, Geert-Jan van Gemert, Gunnar R. Mair, Adriaan M. W. Vermunt, Bruno G. Douradinha, Vera van Noort, et al. 2008. “Proteomic Profiling of Plasmodium Sporozoite Maturation Identifies New Proteins Essential for Parasite Development and Infectivity.” *PLoS Pathogens* 4 (10): e1000195.

Liffner, Benjamin, and Sabrina Absalon. 2021. “Expansion Microscopy Reveals Plasmodium Falciparum Blood-Stage Parasites Undergo Anaphase with A Chromatin Bridge in the Absence of Mini-Chromosome Maintenance Complex Binding Protein.” *Microorganisms* 9 (11): 2306.

———. 2023. “Expansion Microscopy of Apicomplexan Parasites.” *Molecular Microbiology*, August. https://doi.org/10.1111/mmi.15135.

Liffner, Benjamin, Juan Miguel Balbin, Gerald J. Shami, Ghizal Siddiqui, Jan Strauss, Sonja Frölich, Gary K. Heinemann, et al. 2022. “Cell Biological Analysis

Reveals an Essential Role for Pfcerli2 in Erythrocyte Invasion by Malaria Parasites." *Communications Biology* 5 (1): 1–17.

Liffner, Benjamin, Juan Miguel Balbin, Jan Stephan Wichers, Tim-Wolf Gilberger, and Danny W. Wilson. 2021. "The Ins and Outs of Plasmodium Rhoptries, Focusing on the Cytosolic Side." *Trends in Parasitology* 37 (7): 638–50.

Liffner, Benjamin, Ana Karla Cepeda Diaz, James Blauwkamp, David Anaguano, Sonja Frölich, Vasant Muralidharan, Danny W. Wilson, Jeffrey Dvorin, and Sabrina Absalon. 2023. "Atlas of Plasmodium Falciparum Intraerythrocytic Development Using Expansion Microscopy." https://doi.org/10.7554/elife.88088.1.

Liffner, Benjamin, Ana Karla Cepeda Diaz, James Blauwkamp, David Anaguano, Sonja Frolich, Vasant Muralidharan, Danny W. Wilson, Jeffrey D. Dvorin, and Sabrina Absalon. 2023. "Atlas of Plasmodium Falciparum Intraerythrocytic Development Using Expansion Microscopy." *eLife* 12 (December). https://doi.org/10.7554/eLife.88088.

Llinás, Manuel, Zbynek Bozdech, Edith D. Wong, Alex T. Adai, and Joseph L. DeRisi. 2006. "Comparative Whole Genome Transcriptome Analysis of Three Plasmodium Falciparum Strains." *Nucleic Acids Research* 34 (4): 1166–73.

Mageswaran, Shrawan Kumar, Amandine Guérin, Liam M. Theveny, William David Chen, Matthew Martinez, Maryse Lebrun, Boris Striepen, and Yi-Wei Chang. 2021. "In Situ Ultrastructures of Two Evolutionarily Distant Apicomplexan Rhoptry Secretion Systems." *Nature Communications* 12 (1): 4983.

Martinez, Matthew, William David Chen, Marta Mendonça Cova, Petra Molnár, Shrawan Kumar Mageswaran, Amandine Guérin, Audrey R. Odom John, Maryse Lebrun, and Yi-Wei Chang. 2022. "Rhoptry Secretion System Structure and Priming in Plasmodium Falciparum Revealed Using in Situ Cryo-Electron Tomography." *Nature Microbiology*. https://doi.org/10.1038/s41564-022-01171-3.

Ooij, Christiaan van, Pamela Tamez, Souvik Bhattacharjee, N. Luisa Hiller, Travis Harrison, Konstantinos Liolios, Taco Kooij, et al. 2008. "The Malaria Secretome:

From Algorithms to Essential Function in Blood Stage Infection." *PLoS Pathogens* 4 (6): e1000084.

Perrin, Abigail J., Christine R. Collins, Matthew R. G. Russell, Lucy M. Collinson, David A. Baker, and Michael J. Blackman. 2018. "The Actinomyosin Motor Drives Malaria Parasite Red Blood Cell Invasion but Not Egress." *mBio* 9 (4). https://doi.org/10.1128/mBio.00905-18.

Rajaram, Krithika, Hans B. Liu, and Sean T. Prigge. 2020. "Redesigned TetR-Aptamer System To Control Gene Expression in Plasmodium Falciparum." *mSphere* 5 (4). https://doi.org/10.1128/mSphere.00457-20.

Ressurreição, Margarida, James A. Thomas, Stephanie D. Nofal, Christian Flueck, Robert W. Moon, David A. Baker, and Christiaan van Ooij. 2020. "Use of a Highly Specific Kinase Inhibitor for Rapid, Simple and Precise Synchronization of Plasmodium Falciparum and Plasmodium Knowlesi Asexual Blood-Stage Parasites." *PloS One* 15 (7): e0235798.

Riglar, David T., Dave Richard, Danny W. Wilson, Michelle J. Boyle, Chaitali Dekiwadia, Lynne Turnbull, Fiona Angrisano, et al. 2011. "Super-Resolution Dissection of Coordinated Events during Malaria Parasite Invasion of the Human Erythrocyte." *Cell Host & Microbe* 9 (1): 9–20.

Rudlaff, Rachel M., Stephan Kraemer, Jeffrey Marshman, and Jeffrey D. Dvorin. 2020. "Three-Dimensional Ultrastructure of Plasmodium Falciparum throughout Cytokinesis." *PLoS Pathogens* 16 (6): e1008587.

Segev-Zarko, Li-Av, Peter D. Dahlberg, Stella Y. Sun, Daniël M. Pelt, Chi Yong Kim, Elizabeth S. Egan, James A. Sethian, Wah Chiu, and John C. Boothroyd. 2022. "Cryo-Electron Tomography with Mixed-Scale Dense Neural Networks Reveals Key Steps in Deployment of Toxoplasma Invasion Machinery." *PNAS Nexus* 1 (4): gac183.

Sherling, Emma S., Ellen Knuepfer, Joseph A. Brzostowski, Louis H. Miller, Michael J. Blackman, and Christiaan van Ooij. 2017. "The Plasmodium Falciparum Rhoptry

Protein RhopH3 Plays Essential Roles in Host Cell Invasion and Nutrient Uptake." *eLife* 6 (March). https://doi.org/10.7554/eLife.23239.

Sherling, Emma S., Abigail J. Perrin, Ellen Knuepfer, Matthew R. G. Russell, Lucy M. Collinson, Louis H. Miller, and Michael J. Blackman. 2019. "The Plasmodium Falciparum Rhoptry Bulb Protein RAMA Plays an Essential Role in Rhoptry Neck Morphogenesis and Host Red Blood Cell Invasion." *PLoS Pathogens* 15 (9): e1008049.

Vulliez-Le Normand, Brigitte, Michelle L. Tonkin, Mauld H. Lamarque, Susann Langer, Sylviane Hoos, Magali Roques, Frederick A. Saul, et al. 2012. "Structural and Functional Insights into the Malaria Parasite Moving Junction Complex." *PLoS Pathogens* 8 (6): e1002755.

Wang, Kevin, Eric D. Peng, Amy S. Huang, Dong Xia, Sarah J. Vermont, Gaelle Lentini, Maryse Lebrun, Jonathan M. Wastling, and Peter J. Bradley. 2016. "Identification of Novel O-Linked Glycosylated Toxoplasma Proteins by Vicia Villosa Lectin Chromatography." *PloS One* 11 (3): e0150561.

Weiss, Greta E., Paul R. Gilson, Tana Taechalertpaisarn, Wai-Hong Tham, Nienke W. M. de Jong, Katherine L. Harvey, Freya J. I. Fowkes, et al. 2015. "Revealing the Sequence and Resulting Cellular Morphology of Receptor-Ligand Interactions during Plasmodium Falciparum Invasion of Erythrocytes." *PLoS Pathogens* 11 (2): e1004670.

World Health Organization. 2022. *World Malaria Report 2022*. World Health Organization.

Yahata, Kazuhide, Melissa N. Hart, Heledd Davies, Masahito Asada, Samuel C. Wassmer, Thomas J. Templeton, Moritz Treeck, Robert W. Moon, and Osamu Kaneko. 2021. "Gliding Motility of *Plasmodium* Merozoites." *Proceedings of the National Academy of Sciences of the United States of America* 118 (48). https://doi.org/10.1073/pnas.2114442118.

Tables

Table 3.1. List of primers used in the study to generate the cell lines RON11^{apt}.

Amplicon	Primer	Sequence (5' – 3')
RON11-Cterm integration	P1	TGTTTAGGAATTTTTGGAGGTATTTGATAG
Apt integration	P2	CTAGACTAGGTTCCAAGATCTCCC
RON11-Cterm	P3	ATTGTGTATCCCGATATCGATGTTAATAGTTTAAAAAAAATACTAACAG AAGTAAGATG
	P4	CGTCATAAGGGTATCCGGAGACGTCTTTCGAATCAGATGCTGACTGT AAATAAG
RON11-3'UTR	P5	CCAATGGCCCCTTTCCGGGCGCGCCCTTTTTTGTTTGAAATTGGCAA AAATATTAGTAG
	P6	ACTATTAACATCGATATCGGGATACACAATAGAATATTAATTAAGTGTA TTATTAAGTG
RON11 gRNA	P7	CATATTAAGTATATAATATTGATATGGATGTCGAAAGAAAGTTTTAGAG CTAGAAATAGC

Supplemental Figures

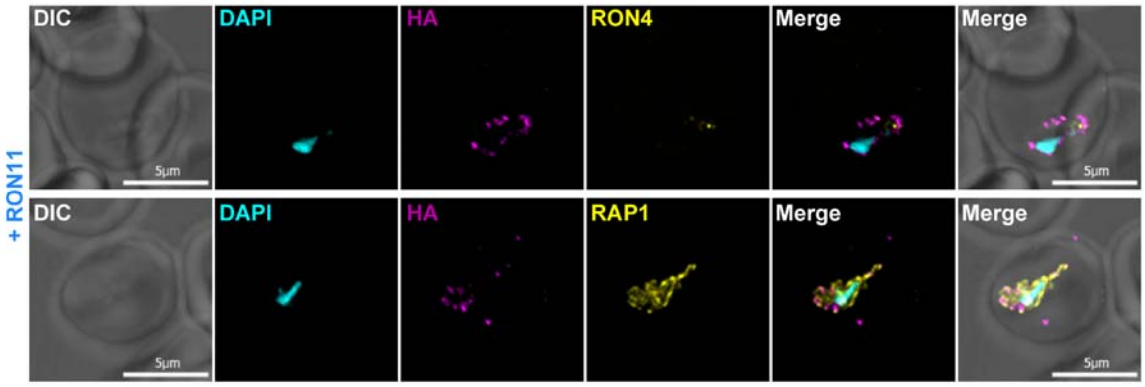

Supplemental figure 1. RON11 localizes to the parasite periphery during early-ring stages. IFAs showing the localization of RON11 in RON11^{apt} rings with respect to the rhoptry markers RON4 and RAP1. Synchronous parasites were fixed with PFA and stained with specific antibodies. Images from left to right are phase-contrast, DAPI (nucleus, cyan), anti-HA (RON11, magenta), anti-RON4 or RAP1 (yellow), and fluorescence merge. Z stack images were deconvolved and projected as a combined single image. Representative images of 2 biological replicates.

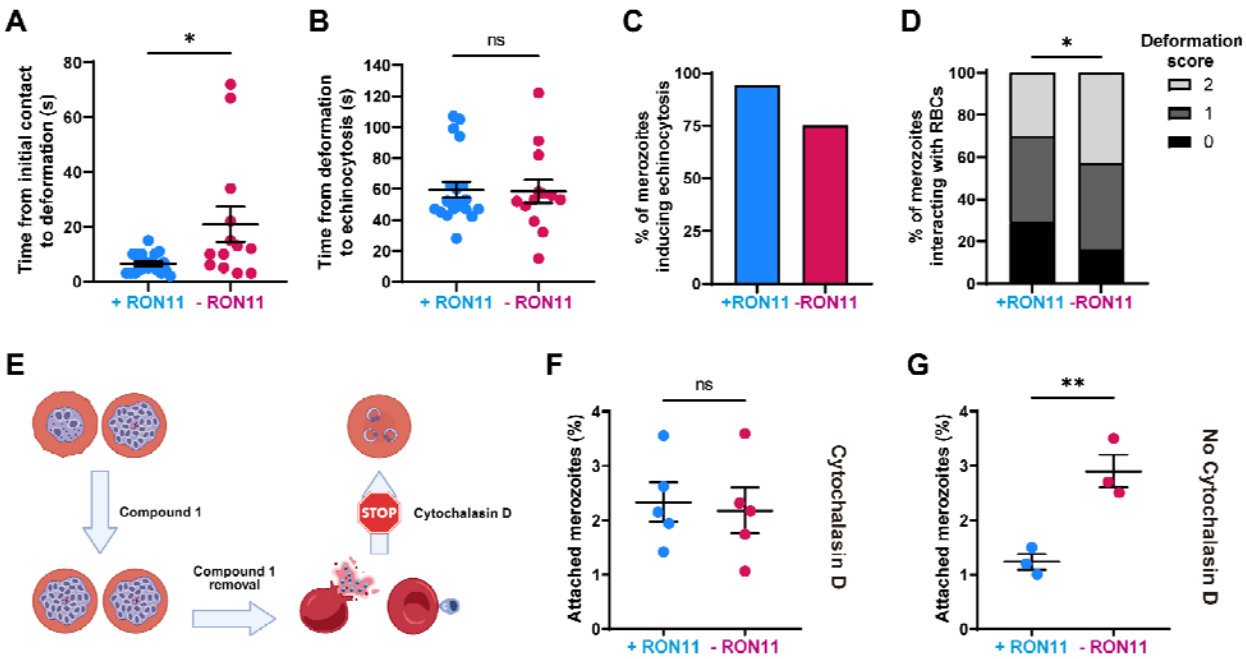

Supplemental figure 2. RON11^{apt} merozoites attached to RBCs in the presence or absence of aTc. **(A)** Duration between first contact of merozoites with RBCs and observation of RBC deformation. (n = 3 biological replicates, 20 merozoites for +RON11 and 13 for -RON11; error bars = SEM; *p < 0.05 by unpaired two-tailed t-test). **(B)** Duration between merozoite first merozoite-induced RBC deformation and echinocytosis. (n = 3 biological replicates, 20 merozoites for +RON11 and 13 for -RON11; error bars = SEM; ns = non-significant by unpaired two-tailed t-test). **(C)** Quantification of RBCs showing echinocytosis after merozoite-induced deformation. (n = 3 biological replicates, 34 merozoites for +RON11 and 44 for -RON11). **(D)** Deformation scores based on the strength of merozoite-RBC interaction. 0 = no deformation; 1 = shallow indentation/membrane pinching; 2 = deeper indentation to the side of RBC/intermediate level of host cell membrane pinching around parasite. (n = 3 biological replicates, 44 merozoites for each condition; *p < 0.05 by chi-squared test). **(E)** Schematic of the actin-polymerization inhibitor assay. Schizonts were tightly synchronized incubating for 4 hours with the PKG inhibitor, Compound 1. After incubation, schizonts were washed twice and then transferred to fresh red blood cells in the presence of the actin inhibitor, cytochalasin D, for 30 minutes. Created with BioRender.com. **(F and G)** Quantification of RON11^{apt} merozoites attached to RBCs in the presence or absence of aTc, after incubation with **(F)** or without **(G)** cytochalasin D. Parasites were smeared 30 minutes after Compound 1 removal,, stained with Hema 3, and scored by light microscopy. Attached-merozoites were blindly scored and represented as the percentage of events per 100 RBCs (n = 5 and 3 biological replicates respectively; error bars = SEM; ns = non-significant; **p < 0.01 by unpaired two-tailed t-test).

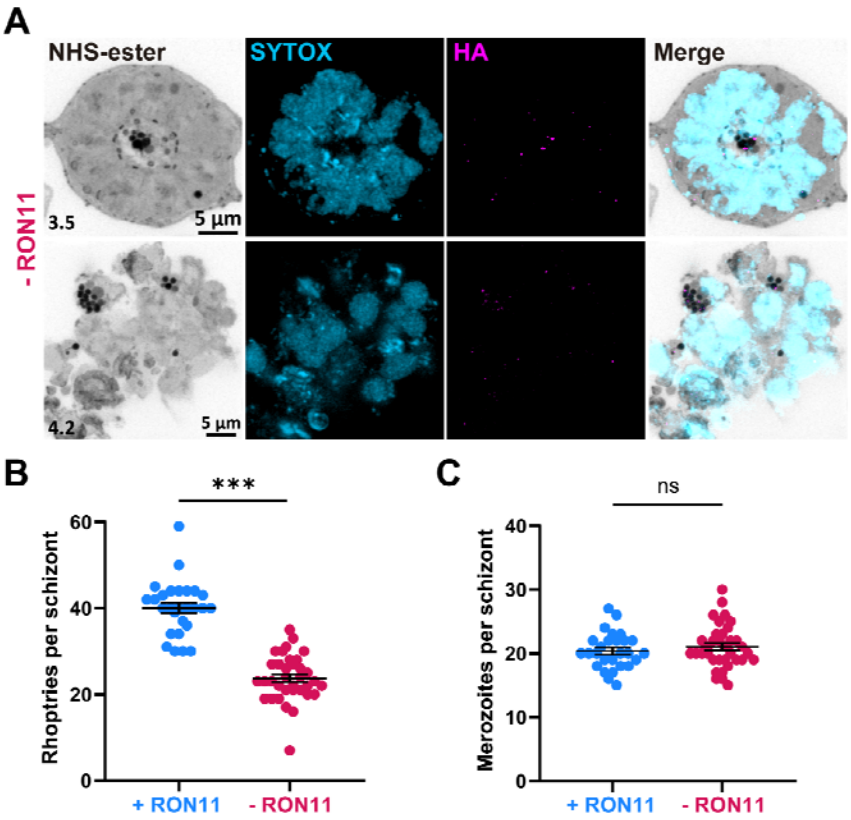

Supplemental figure 3. RON11 knockdown can generate multiple rhoptries but does not affect the number of merozoites. (A) Representative images of RON11^{apt} parasite showing multiple rhoptries accumulating within fully developed schizonts in the absence of aTc. ML10-arrested parasites were expanded by U-ExM, fixed with PFA, and stained with NHS-Ester (greyscale), anti-HA (magenta), and the DNA dye SYTOX (cyan). Selected Z stack images were projected as a combined single image. Number on image = Z-axis thickness of projection in µm. **(B and C)** Quantification of **(B)** rhoptries per merozoites and **(C)** merozoites per schizont in the presence and absence of aTc. (n = 4 biological replicates, 28 schizonts for +RON11 and 36 for -RON11; error bars = SEM; ns = non-significant; ***$p < 0.001$ by unpaired two-tailed *t*-test)

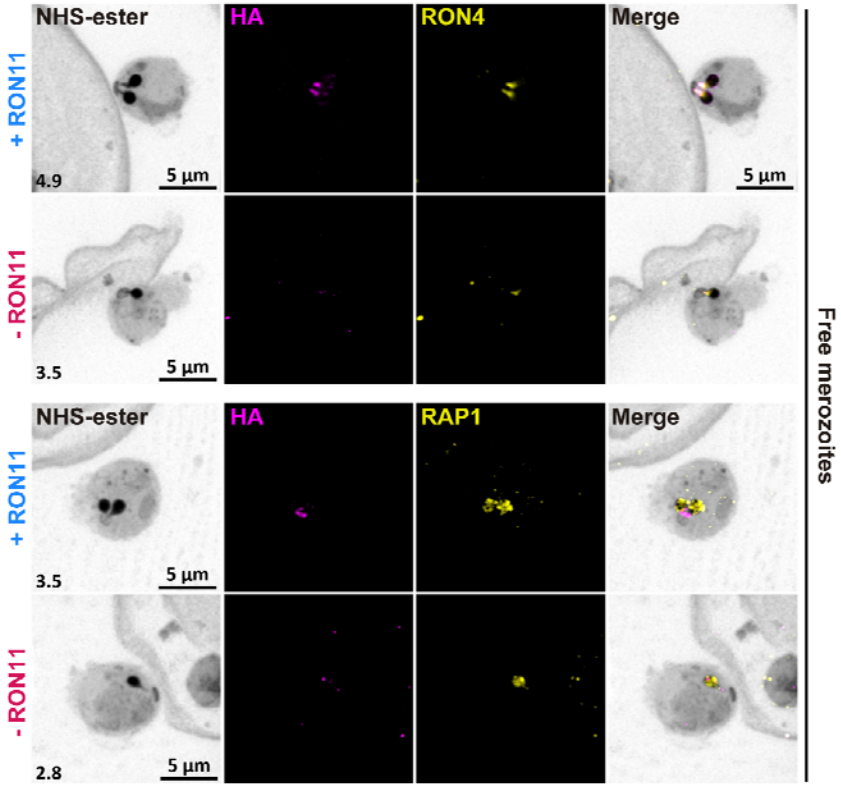

Supplemental figure 4. RON11 knockdown does not affect the localization of other rhoptry proteins in single rhoptry merozoites. Representative images of RON11^{apt} free merozoites showing the localization of RON11 with respect to RON4 and RAP1 in the presence and absence of aTc. Late-schizonts were expanded by U-ExM, fixed with PFA, and stained with NHS-Ester (greyscale), anti-HA (magenta), and anti-RON4 or RAP1 (yellow). Selected Z stack images were projected as a combined single image. Number on image = Z-axis thickness of projection in µm.

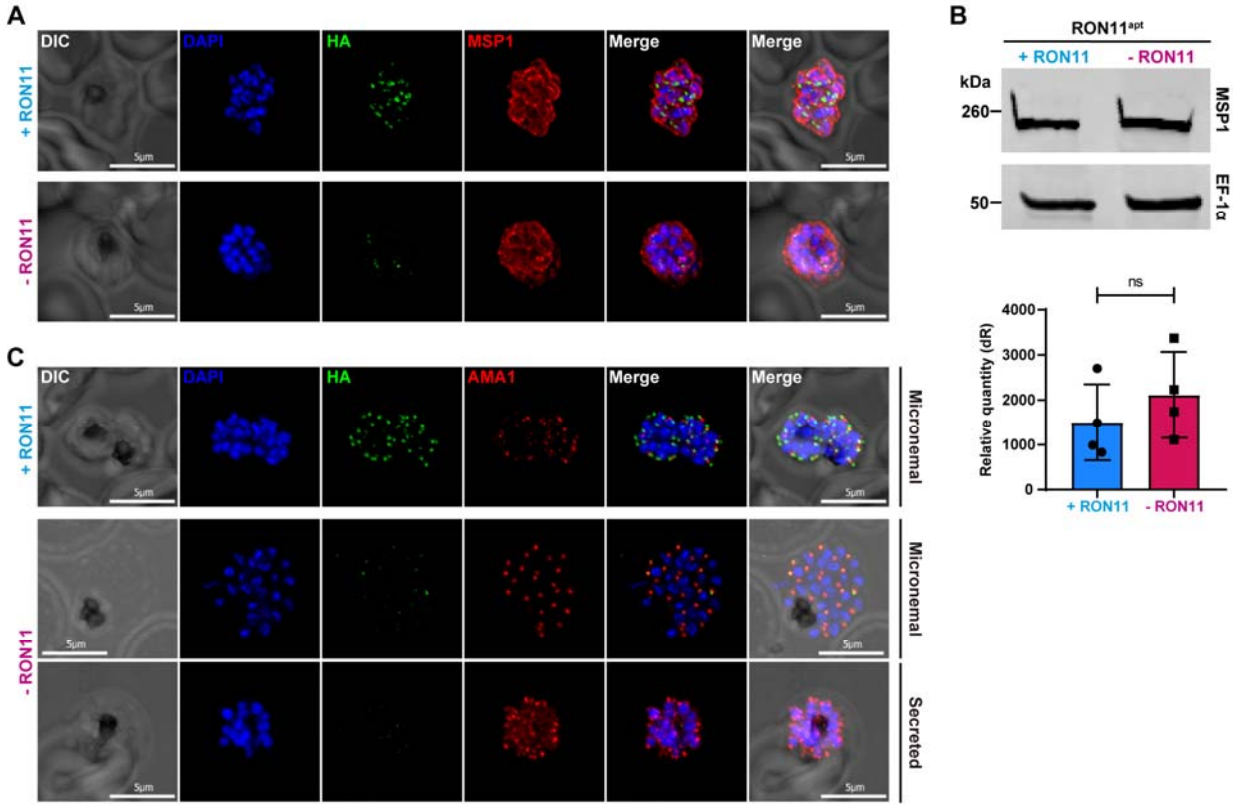

Supplemental figure 5. RON11 knockdown does not impact the expression and secretion of MSP1 and AMA1. (A) Representative IFAs of RON11^{apt} schizonts showing secretion of MSP1 proteins in the presence or absence of aTc. E64-arrested schizonts were fixed with PFA and stained with specific antibodies. Images from left to right are phase-contrast, DAPI (nucleus, blue), anti-HA (RON11, green), anti-MSP1 (red), and fluorescence merges. Z stack images were deconvolved and projected as a combined single image. Representative images of 3 biological replicates. **(B)** (Top) Western blot of parasite lysates isolated from E64-arrested RON11^{apt} parasites in the presence and absence of aTc. Samples were probed with antibodies against MSP1 and EF1α (loading control). The protein marker sizes are shown on the left. Representative blot of 4 biological replicates shown. (Bottom) Quantification of the relative level of MSP1 total protein content in E64-arrested RON11^{apt} parasites in the presence and absence of aTc. Band intensities were normalized to the loading control, EF1α, and are presented as normalized arbitrary units (A.U.) (n = 4 biological replicates; error bars = SD; ns = non-significant by unpaired two-tailed t-test). **(C)** Representative IFAs of RON11^{apt} schizonts showing AMA1 localization in the presence or absence of aTc. E64-arrested schizonts were fixed with PFA and stained with specific antibodies. Images from left to right are phase-contrast, DAPI (nucleus, blue), anti-HA (RON11, green), anti-AMA1 (red), and fluorescence merges. Z stack images were deconvolved and projected as a combined single image. Representative images of 3 biological replicates.

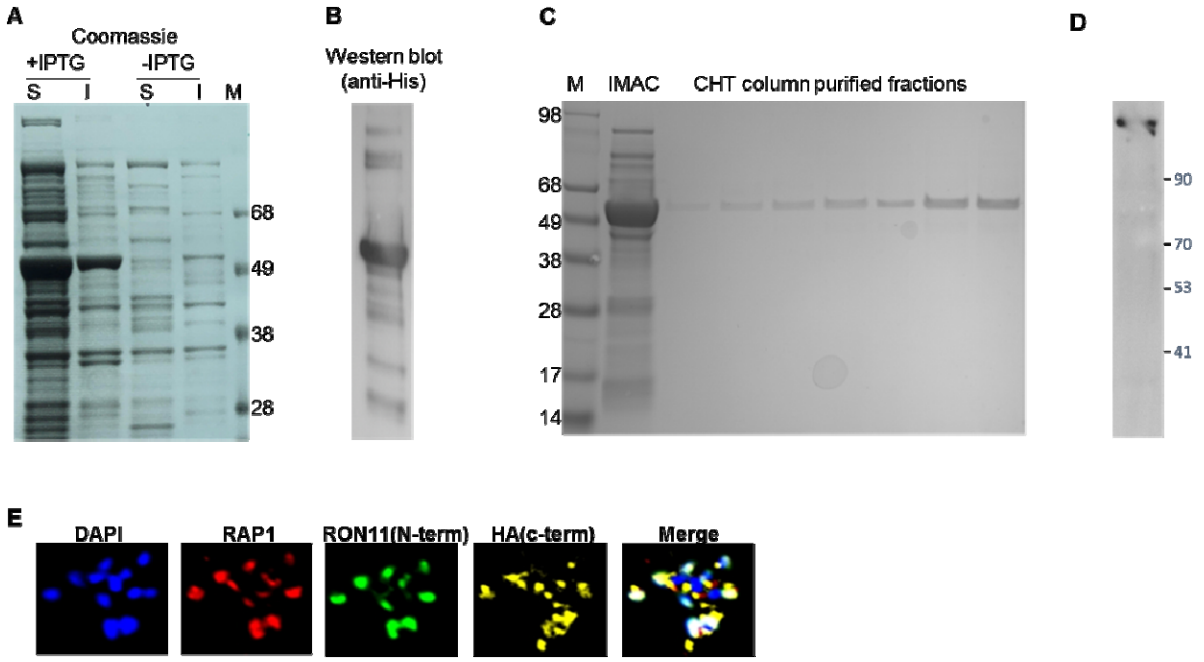

Supplemental figure 6. Expression and purification of recombinant RON11, and validation of anti-RON11 antibody. (A) Expression of rMBP-RON11 (aa 32-442) protein in *E.coli*. Soluble (S) and insoluble (I) fractions from cell lysates without and without IPTG induction. M; Marker. **(B)** Western blot analysis of the soluble fraction using anti-His antibody and detected using anti-mouse HRP conjugated secondary antibody. **(C)** rMBP-RON11 following IMAC purification and subsequent clean-up using CHT column. **(D)** Western blot analysis of P.falciparum schizont lysates using anti-RON11 antibody. **(E)** Immunofluorescence microscopy of mature schizont stained with DAPI, anti-RON11 (N-term), anti-HA (c-term) and anti-RAP1 antibodies.